Phospholipid Scramblase-1 controls efficient neurotransmission and synaptic vesicle retrieval at cerebellar synapses

Phospholipid Scramblase-1 controls efficient neurotransmission and synaptic vesicle retrieval at cerebellar synapses

Margherita Caputo[1], Daniela Ivanova[2,3], Sylvette Chasserot-Golaz[1], Frédéric Doussau[1], Anne-Marie Haeberlé[1], Cathy Royer[5], Sebahat Ozkan[1], Jason Ecard[1], Nicolas Vitale[1§], Michael A.Cousin[2,3,4], Petra Tóth[1§], Stéphane Gasman[1#§] and Stéphane Ory[1#§]

# S. Gasman and S. Ory contributed equally to this paper
§ Corresponding authors: Petra Tóth (petra.toth@inci-cnrs.unistra.fr), Nicolas Vitale (vitalen@inci-cnrs.unistra.fr), Stéphane Gasman (sgasman@inci-cnrs.unistra.fr) and Stéphane Ory (ory@ inci-cnrs.unistra.fr)

1- Centre National de la Recherche Scientifique, Université de Strasbourg, Institut des Neurosciences Cellulaires et Intégratives, F-67000, Strasbourg, France
2- Centre for Discovery Brain Sciences, Hugh Robson Building, George Square, University of Edinburgh, Edinburgh, Scotland, EH8 9XD, UK
3- Muir Maxwell Epilepsy Centre, Hugh Robson Building, George Square, University of Edinburgh, Edinburgh, Scotland, EH8 9XD, UK
4- Simons Initiative for the Developing Brain, Hugh Robson Building, George Square, University of Edinburgh, Edinburgh, Scotland, EH8 9XD, UK
5- Plateforme Imagerie In Vitro, Centre National de la Recherche Scientifique, UPS3256, F-67000, Strasbourg, France

Running title: PLSCR1 controls synaptic transmission

Number of pages: 34
Number of figures: 6
Number of table: 2
Number of words: Abstract: 160; Introduction: 740; Discussion: 1338

The authors declare no competing financial interests.

Acknowledgements

This work was financially supported by the Agence Nationale pour la Recherche ("LipidTrans4NeuroTraffic", N° ANR-19-CE16-0012-01) to SG; by a fellowship from la Fondation pour la Recherche Médicale (n° FDT202106013135) and a travel grant from The Company of Biologists (n° JCSTF1911344) to MC; and by the Wellcome Trust Investigator Award to MAC (204954/Z/16/Z). For open access, authors have applied a CC-BY public copyright license to any accepted manuscript version arising from this submission. INSERM is providing salary to SCG, SG and NV. We acknowledge the Plateforme Imagerie In Vitro at CNRS UPS3256, Dr Jean-Daniel Fauny (IBMC, UPR3512, Strasbourg) for technical assistance with live cell imaging microscopy set up and the animal facility of Chronobiotron (UMS 3415). The authors are grateful to Charlotte Caquineau and Audrey Groh for technical assistance.

Abstract

Phospholipids are asymmetrically distributed at the plasma membrane. This asymmetric lipid distribution is transiently altered during calcium-regulated exocytosis but the impact of this transient remodeling on presynaptic function is currently unknown. As PhosphoLipid SCRamblase 1 (PLSCR1) randomizes phospholipid distribution between the two leaflets of the plasma membrane in response to calcium activation, we set out to determine its role in neurotransmission. We report here that PLSCR1 is expressed in cerebellar granule cells (GrCs) and that PLSCR1-dependent phosphatidylserine egress occurred at synapses in response to neuron stimulation. Synaptic transmission is impaired at GrC *Plscr1*$^{-/-}$ synapses and both PS egress and synaptic vesicle endocytosis are inhibited in *Plscr1*$^{-/-}$ cultured neurons from male and female mice, demonstrating that PLSCR1 controls phospholipid asymmetry remodeling and synaptic vesicle retrieval following neurotransmitter release. Altogether, our data reveal a novel key role for PLSCR1 in synaptic vesicle recycling and provide the first evidence that phospholipid scrambling at the plasma membrane is a prerequisite for optimal presynaptic performance.

Keywords: lipid scrambling, PLSCR1, calcium-regulated exocytosis, compensatory endocytosis, neurotransmission, pHluorin, neurons

Significance statement

During calcium-regulated exocytosis, phospholipids like phosphatidylserine (PS) undergo dynamic remodeling. Phospholipid Scramblase-1 (PLSCR1) belongs to a family of proteins able to randomize lipids at the cell surface in response to intracellular Ca^{2+} increases. Whether PLSCR1 and PS egress have a role during neurotransmission is unknown. We show that PLSCR1 expression is restricted to specific brain regions capable of sustaining neurotransmission during high firing rates. In the absence of PLSCR1, synaptic transmission is impaired, and both PS egress and synaptic vesicle endocytosis are hindered. This study highlights the pivotal role of PLSCR1 in regulating optimal presynaptic performance by redistributing phospholipid at the plasma membrane to control compensatory endocytosis.

Introduction

Phospholipids (PLs) at the plasma membrane are asymmetrically distributed by energy-dependent transporters, which move phosphatidylethanolamine (PE) and phosphatidylserine (PS) from the extracellular to the cytoplasmic leaflet (flippases) and, conversely, phosphatidylcholine (PC) from the cytoplasmic to the extracellular leaflet (floppases). PS and PE are therefore virtually absent from the outer leaflet of the plasma membrane (Zachowski, 1993; Kobayashi and Menon, 2018; Clarke et al., 2020). This homeostatic and asymmetric lipid distribution is disrupted in several biological processes resulting in PS exposure at the extracellular leaflet. Cell surface PS exposure is massive and irreversible during events such as apoptosis or platelet activation which is required for thrombosis (Bevers and Williamson, 2016). In contrast during regulated exocytosis in either immune or neuroendocrine cells, PS egress is transient and strictly restricted to sites of membrane fusion (Martin et al., 2000, 2000; Vitale et al., 2001; Kato et al., 2002; Malacombe et al., 2006; Ory et al., 2013; Rysavy et al., 2014; Audo et al., 2017).

Whether massive or limited, the loss of plasma membrane asymmetry is mainly due to the activation of phospholipid scramblases which randomize PLs across the plasma membrane (Daleke, 2003; Kobayashi and Menon, 2018). Phospholipid scramblase-1 (PLSCR1), originally isolated from erythrocytes, was the first scramblase identified able to reproduce lipid scrambling in response to Ca^{2+} increases when introduced into liposomes (Bassé et al., 1996; Zhou et al., 1997). PLSCR1 also controls PS egress in response to mast cell and chromaffin cell

stimulation (Kato et al., 2002; Amir-Moazami et al., 2008; Smrž et al., 2008; Ory et al., 2013). However, preventing PS egress by suppressing PLSCR1 expression leads to different functional outcomes. For example, the release of secretory granule contents by exocytosis is reduced in mast cells (Amir-Moazami et al., 2008), but unaltered in chromaffin cells (Ory et al., 2013) which instead show defective compensatory endocytosis, preventing secretory granule protein retrieval (Ory et al., 2013). Therefore, the leaflet organization of the lipids at the plasma membrane and/or PLSCR1 control exocytosis and/or endocytosis in secretory cells. However, the mechanism of lipid scrambling by PLSCR1 is currently a matter of debate. This is because PLSCR1 is a single pass transmembrane protein that cannot form a channel to transport PLs, and the deletion of *Plscr1* gene in mice does not alter plasma membrane PS egress either in activated platelets or in response to apoptosis (Zhou et al., 2002). Nonetheless, the identification of additional scramblases, namely TMEM16F and XKR-8 controlling extracellular PS exposure during platelet activation (Suzuki et al., 2010; Yang et al., 2012) and apoptosis (Suzuki et al., 2013), respectively, provides evidence that, despite their common ability to collapse lipid asymmetry, scramblases can regulate distinct mechanisms at the plasma membrane.

Neuronal communication relies on the release of neurotransmitters at synapses, which occurs by Ca^{2+}-dependent exocytosis of synaptic vesicles (SVs), resulting in the insertion of SV membrane into the presynaptic plasma membrane. To support high rates of release during synaptic transmission, SV components must be retrieved rapidly by compensatory endocytosis to preserve plasma membrane homeostasis, to clear exocytic sites for the recruitment of release-ready SVs and to replenish the releasable SV pool (Wu et al., 2014; Maritzen and Haucke, 2018; Chanaday et al., 2019). Activity-dependent SV fusion and retrieval are spatially and temporally coupled within nerve terminals and dysfunction in either process is increasingly associated with pathologies including epilepsy, autism or intellectual disability (Bonnycastle et al., 2021). The molecular mechanisms coupling endocytosis to exocytosis have been extensively studied in neurons (Maritzen and Haucke, 2018; Bolz et al., 2023; Wu and Chan, 2024). However, although exocytosis and endocytosis imply successive reorganization of PLs belonging to separate membrane compartments, little attention has been paid to the role of plasma membrane PLs in these events.

The present study sought to determine whether SV recycling relied on PLSCR1, and whether neurotransmission was influenced by its loss. Through a combination of approaches including immunofluorescence on primary cerebellar cultures, electron microscopy and electrophysiology on acute cerebellar slices from both wild-type (*Plscr1*$^{+/+}$) and *Plscr1* knock-

out mice (*Plscr1*$^{-/-}$), we revealed that PLSCR1 activity at synapses is essential for maintaining efficient neurotransmission. Moreover, optical live cell imaging of pHluorin probes revealed that compensatory endocytosis was altered in PLSCR1$^{-/-}$ neurons. Taken together, our data unveil a pivotal role of PLSCR1 in mediating stimulation-dependent PS egress at excitatory synapses. Furthermore, our study provides the first evidence of the impact of PLSCR1-dependent PS egress on facilitating SV recycling and sustaining synaptic transmission during periods of high frequency stimulation.

Material and Methods

Animals and genotyping

Neuronal cells and brain tissues were obtained from *Plscr1*$^{-/-}$ and wild type mice. *Plscr1*$^{+/-}$ mice were purchased from CDTA (Cryopréservation, Distribution, Typage et Archivage animal) housed and raised at Chronobiotron UMS 3415. All mice were bred, handled, and maintained in agreement with European council directive 86/609/EEC and resulting French regulation. Animal work in Edinburgh was performed in accordance with the UK Animal (Scientific Procedures) Act 1986, under Project and Personal License authority and was approved by the Animal Welfare and Ethical Review Body at the University of Edinburgh (Home Office project license to M. Cousin – 70/8878). Animals were killed by schedule 1 procedures in accordance with UK Home Office Guidelines. Animals used in France were handled according to French regulations. P6 to P7 mice pups were killed by anaesthetic overdose, with death confirmed via the destruction of the brain and adult mice were euthanized by cervical dislocation. *Plscr1*$^{+/+}$ and *Plscr1*$^{-/-}$ mice were maintained as heterozygous breeding pairs and genotyped by duplex PCR using 5'-CTACACTGACCTTTAATCAGAGCAG-3', 5'- CCATGTCTGCCCAAGTTCACTCTC-3', and 5'- GCAGCGCATCGCCTTCTATC-3' primers to detect the presence of a 261 bp or a 311 bp fragment for the wild-type or mutant allele respectively. The PCR program was set at 95°C for 3 min; 30 cycles (95°C for 30 sec, 60°C for 30 s,72°C for 30 sec) followed by 10 min elongation at 72°C.

Cell culture, transfection and plasmids

Cerebellar granule (GrCs) cultures were prepared as previously described (Cheung and Cousin, 2011). Briefly, primary cultures of cerebellar neurons were prepared from the cerebella of 6-7 days old C57BL/6J *Plscr1*$^{-/-}$ pups and their littermate controls. After removal, cerebella were placed in HH solution (Table 1), minced up with tweezers and then incubated in Trypsin solution (2T; Table 1) at 37°C for 20 min. After digestion with trypsin, an equal volume of Neutralization solution (N; Table 1) was added to the suspension and the sample was centrifuged at 150 × *g* for 60 s. The supernatant was removed and the pellet suspended in 1 mL of N solution before being triturated using 1000 µL pipette until the solution reached homogeneity. The cell suspension was centrifuged at 340 × *g* for 2 min and the pellet

resuspended in 1.5 mL of DMEM/FCS medium (DFM) (Table 1) and plated as one spot/well at a density of 5–10 × 10^6 cells/coverslip coated with poly-D-lysine (20 μg/mL) diluted in boric acid (100 mM, pH 8.5). After 1 h, wells were flooded with Neurobasal growth medium (NKB) (Table 1) containing 25 mM KCl. The following day, cultures were further supplemented with 1 μM cytosine β-D-arabinofuranoside to inhibit glial cell proliferation. 4 or 5 days after seeding, cells were transfected with Lipofectamine 2000 as described by Nicholson-Fish et al. (2015). Briefly, cells were preincubated in 2 mL of MEM (Thermo Fisher) in 10% CO_2 for 30 min at 37°C, and then transfected for 2 h with a complex containing 2 μL of Lipofectamine and 1 μg of the indicated plasmids/well. Cells were subsequently washed with MEM before replacement with conditioned Neurobasal media. Cells were imaged 48 h post-transfection.

Synaptophysin-pHluorin was a gift from Prof. L. Lagnado (University of Sussex, Brighton, U K) and GFP-PLSCR1 plasmids were previously described (Granseth et al., 2006; Ory et al., 20 13). The mCherry-PLSCR1 constructs were obtained by PCR using the mouse *Plscr1* as a tem plate. Amplified fragments were subcloned in pmCherry-C1 vectors between BglII and EcoRI restriction sites using forward 5'-CAGATCTGAAAACCACAGCAAGCAAAC-3' and revers e primer 5' –GGAATTCTTACTGCCATGCTCCTGATC-3'.

Table 1: Solutions for CGN preparation

HH Solution	HBSS Ca^{2+}/Mg^{2+} free (Sigma, H6648) supplemented with 5 mL of 1M sterile Hepes pH 7.3
Trypsin Solution (2T)	1 mL of sterile 5mg/mL trypsin in 9 mL of HH to make final 0.05% solution
DFM medium	DMEM high glucose (Thermo Fisher, 41966029) supplemented with 10% FCS and 1% Pen/Strep
Neutralization Solution (N)	1 mL of sterile DNase containing 1200 U in 19 mL of DFM to make final 60U/mL solution
NBK medium	Neurobasal (Thermo Fisher 21103049) supplemented with 2% B27, 0.25% 200 mM Glutamine and 1% Pen/Strep

Table 2

Reagents					
Type	**Name**	**Company**	**Reference**	**Dilution**	**RRID**
Antibody	Rabbit anti Synaptotagmin1	Synaptic systems	105103	1/1000	AB_11042157
Antibody	Guinea pig anti vGlut1	Synaptic systems	135304	1/500	AB_887878
Antibody	Mouse anti Synaptophysin	Sigma	S5768	1/500	AB_477523
Antibody	Rabbit anti-GFP	Abcam	ab290	1/1000	AB_303395
Antibody	Mouse anti actin	Sigma	A5441	1/1000	AB_476744
Antibody	Mouse anti PLSCR1	Proteintech	11582-1AP	1/500	AB_2165659
Antibody	Mouse anti PSD95	Thermofisher scientific	MA1-045	1/500	AB_325399
Antibody	HRP-conjugated goat anti-mouse and anti-rabbit	PerBio	31430, 31460	1/50000	AB_228307, AB_228341
Antibody	Alexa Fluor647®-conjugated goat anti guinea pig	Thermofischer scientific	A21450,	1/1000	AB_2735091
Antibody	Alexa Fluor555®-conjugated goat anti rabbit	Thermofischer scientific	A21428	1/1000	AB_2535849
Antibody	Gold particle-conjugated anti-rabbit and anti guinea pig	Aurion	810 144, 825.011	1/100	N/A
Chemicals	TMR-Phalloidin	Sigma	P1951	1/1500	AB_2315148
Chemicals	AnxA5 gold conjugate protein	Biobyt	Orb170087	1/50	N/A

Chemicals	AnxA5-Alexa Fluor 647®	Biolegend	640911	1/50	N/A
Chemicals	Hoechst	Thermoscientific	33342	1/10000	N/A
Chemicals	Pictotoxin	Abcam	Ab120315	100 mM in ACSF	N/A
Chemicals	CGP52432	Abcam	Ab120330	10 mM in ACSF	N/A
Chemicals	D-AP5	Abcam	Ab120003	100 mM in ACSF	N/A
Chemicals	AM251	Abcam	Ab120088	1 mM in ACSF	N/A

Immunofluorescence, Confocal microscopy and Image analysis

Neurons were fixed with ice-cold 4% (w/v) paraformaldehyde in phosphate buffered saline (PBS) for 10 min at room temperature and permeabilized with 0.1% v/v Triton® X-100 in PBS for 4 min. The cells were washed with PBS, blocked with 3% BSA in PBS and 5% Goat Serum (Sigma, #G9023) for 1 h before being incubated with primary antibodies in 3% BSA in PBS for 1 h. Then cells were labelled with secondary antibodies coupled to fluorescent Alexa Fluor dyes (see Table 2 for antibodies list and references). Actin was stained with Tetramethyl-rhodamineB coupled Phalloidin (TMR-phalloidin, Table 2) and nuclei were stained with 1 µg/mL Hoechst (Thermo Scientific, 33342). Cells were observed under a confocal microscope equipped with continuous laser emitting at 405, 488, 561 and 633 nm (SP5, Leica Microsystems), using a 63× objective (NA 1.4). Individual wavelengths Fluorophore emission at individual wavelength was sequentially acquired and performed with an acousto-optical beam set to 415-470, 498-520, 571-610 and 643-720 nm depending on the fluorophore detected.

Annexin-A5 (AnxA5) staining was performed as described before (Ory et al., 2013). Cerebellar granule cells were hyperpolarized for 10 min in Imaging Buffer (170 mM NaCl, 3.5 mM KCl, 0.4 mM KH_2PO_4, 20 mM TES (N-tris (hydroxyl-methyl)-methyl-2-aminoethane-sulfonic acid), 5 mM $NaHCO_3$, 5 mM glucose, 1.2 mM $MgCl_2$, and 1.3 mM $CaCl_2$, pH 7.4). Neurons were then maintained for 10 min at 37°C in the presence of AlexaFluor®-647-conjugated AnxA5 (1/50, Biolegend) in resting solution (Locke's solution: 140 mM NaCl, 4.7 mM KCl, 2.5 mM $CaCl_2$, 1.2 mM KH_2PO_4, 1.2 mM $MgSO_4$, 11 mM glucose, and 15 mM HEPES, pH 7.2) or in

stimulation solution containing 50 mM K^+ (Locke's solution containing 50 mM KCl and 89 mM NaCl). Neurons were then fixed and counterstained for 30 min with TMR-phalloidin. To identify PS egress sites, cells were incubated in culture medium containing 30 mM KCl and both Alexa Fluor®-647-conjugated AnxA5 and anti-Synaptotagmin1 (Syt1) antibody directed against the luminal domain. Cells were then fixed and Syt1 antibodies revealed with a goat anti-rabbit antibody conjugated to AlexaFluor® 555. AnxA5 and Syt1 staining were observed under confocal microscope (SP5, Leica Microsystems). Image analyses were performed with Icy software. HKmeans thresholding method (Manich et al., 2020) was used to segment actin staining and mean AnxA5 intensity was computed in the resulting region of interest (ROI) delineating the neuronal shape. AnxA5 mean intensity was obtained from 10 fields of view per each independent experiments (n=3).

Preparation of Synaptosomal Fraction

Synaptosomal fractions were prepared as previously described (Dunkley et al., 2008a). Briefly, cerebella from adult mice were collected in an isotonic Sucrose/EDTA buffer (0.32 M Sucrose, 1 mM EDTA, 5 mM Tris-HCl, pH 7; Homogenizing Buffer) and dissociated by applying 13 even strokes with a dounce homogenizer. After centrifugation of the homogenates (1000 x *g*, 10 min, 4°C), the supernatant (S1, Crude extract) was kept on ice and the pellet was resuspended in homogenizing buffer, subjected to additional 17 even strokes and centrifuged (1000 x *g*, 10 min, 4°C). The pellet was discarded and the supernatant S2 was pooled with S1. Protein concentration was measured and adjusted with ice-cold homogenizing buffer to 4-5 mg/mL. Crude extract was loaded onto a discontinuous Percoll gradient (3%, 10%, 15% and 23% Percoll (vol/vol)) and centrifuged at 31,000 x g for 5 min, at 4°C. Each fraction was individually recovered and fractions 3 and 4 enriched in synaptosomes were pooled. Synaptosomes were then diluted in ice-cold homogenizing buffer and centrifuged at 20,000 x g for 30 min at 4°C to concentrate the synaptosomes into the pellet and remove Percoll. Synaptosomes were resuspended in lysis buffer (Cell Extraction Buffer: 10 mM Tris-HCl, pH 7.4, 100 mM NaCl, 1 mM EDTA, 1 mM EGTA, 1 mM NaF, 20 mM $Na_4P_2O_7$, 2 mM Na_3VO_4, 1 % Triton® X-100, 10 % glycerol, 0.1 % SDS, 0.5 % deoxycholate; Invitrogen, #FNN0011) supplemented with protease and phosphatase inhibitor cocktail (Sigma-Aldrich, # P8340) and further subjected to Western Blot analysis.

Western Blotting

Cells and tissues were lysed in cell extraction buffer with protease and phosphatase inhibitor cocktail (Sigma-Aldrich, #P8340,). Cell lysates were cleared at 20,000 g for 10 min at 4°C and protein concentration determined using BioRad protein assay. Proteins (20 µg total) were separated on Novex 4-12% Bis-Tris gels (ThermoFisher Scientific) and transferred to nitrocellulose membrane (BioRad, #1704156). Blots were blocked for 1 h at room temperature in Tris-buffered saline containing 5% (w/v) milk powder (fat free) and 0.1% Tween-20 (TBST; 0.1% Tween, 150 mM NaCl, 10 mM Tris-HCl, pH 7.5) and probed with the anti-PLSCR1, anti-Synaptotagmin1 or anti-PSD95 antibodies (see Table 2). After three washes, blots were incubated with the corresponding secondary antibodies coupled to HRP (Table 2). When possible and when primary antibodies were from different species, blots were incubated with 0.02% sodium azide in TBS-T for 1 h at room temperature to inactivate HRP. Blots were then processed to reveal a second protein on the same blot. Detection was carried out with Prime Western Blotting System (ThermoFisher Scientific) and immunoreactive bands were imaged using Amersham Imager 680 RGB camera System (GE healthcare Life Sciences). Values were normalized to the corresponding β-actin protein levels.

Acute slice preparation and electrophysiological recordings

Slice preparation and electrophysiology recording were performed as previously described (Doussau et al., 2017). Acute horizontal cerebellar slices were prepared from male and female C57Bl/6 mice of both genotype (*Plscr1*$^{+/+}$ and *Plscr1*$^{-/-}$) aged 18-30 days. Mice were anesthetized by isoflurane inhalation (4%) and decapitated. The cerebellum was dissected out in ice-cold artificial cerebrospinal fluid (ACSF) bubbled with carbogen (95% O_2, 5% CO_2) and containing 120 mM NaCl, 3 mM KCl, 26 mM $NaHCO_3$, 1.25 mM NaH_2PO_4, 2.5 mM $CaCl_2$, 2 mM $MgCl_2$, 10 mM glucose and 0.05 mM minocyclin. Slices were then prepared (Microm HM650V) in an ice-cold solution containing 93 mM *N*-Methyl-D-Glucamine, 2.5 mM KCl, 0.5 mM $CaCl_2$, 10 mM $MgSO_4$, 1.2 mM NaH_2PO_4, 30 mM $NaHCO_3$, 20 mM HEPES, 3 mM Na-Pyruvate, 2mM Thiourea, 5 mM Na-ascorbate, 25 mM D-Glucose and 1 mM Kynurenic acid (Zhao et al., 2011). Slices (300 µm thick) were maintained in bubbled ASCF medium (see above) at 34°C until their use for experiments.

After at least 1 h of recovery at 34°C, a cerebellar slice was transferred to a recording chamber. In order to block inhibitory transmission, postsynaptic plasticity, $GABA_B$ and endocannabinoid signaling, slices were continuously perfused with bubbled ACSF containing blockers of $GABA_A$, $GABA_B$, NMDA, CB1 and mGluR1 receptors. To do so, the following

antagonists were added (see Table 2 for references): 100 µM picrotoxin, 10 µM CGP52432 (3-[[(3,4-Dichlorophenyl)-methyl]amino]propyl(diethoxymethyl)phosphinic acid), 100 µM D-AP5 (D-(-)-2-Amino-5-phosphonopentanoic acid) and 1 µM AM251 (1-(2,4-Dichlorophenyl)-5-(4-iodophenyl)-4-methyl-N-(piperidin-1-yl)-1H-pyrazole-3-carboxamide) and 2 µM JNJ16259685((3,4-Dihydro-2H-pyrano[2,3-b]quinolin-7-yl)-(cis-4-methoxycyclohexyl)-methanone). Recordings were made at 34°C in Purkinje cells (PCs) located in the vermis. PCs were visualized using infrared contrast optics on an Olympus BX51WI upright microscope. Whole-cell patch-clamp recordings were obtained using a Multiclamp 700A amplifier (Molecular Devices). Pipette (2.5-3 MΩ resistance) capacitance was cancelled and series resistance (R_s) between 5 and 8 mΩ was compensated at 80%. R_s was monitored regularly during the experiment and the recording was stopped when R_s changed significantly (> 20%). PCs were held at -60 mV. The intracellular solution for voltage-clamp recording contained 140 mM $CsCH_3SO_3$, 10 mM phosphocreatine, 10 mM HEPES, 5 mM QX314-Cl, 10 mM BAPTA, 4 mM Na-ATP and 0.3 mM Na-GTP. Beams of parallel fibers were stimulated extracellularly using a monopolar glass electrode filled with ACSF, positioned at least 100 µm away from the PC to ensure a clear separation between the stimulus artifact and EPSCs. Pulse trains were generated using an Isostim A320 isolated constant current stimulator (World Precision Instruments) controlled by WinWCP freeware (John Dempster, Strathclyde Institute of Pharmacy and Biomedical Sciences, University of Strathclyde, UK). The synaptic currents evoked in PCs were low-pass filtered at 2 KHz and sampled at 20 to 50 KHz (National Instruments).

Cerebellum slices and plasma membrane sheets preparation for transmission electron microscopy.

Wild-type (n = 3) and *Plscr1*$^{-/-}$ (n=3) mice were anesthetized with a mixture of ketamine (100 mg/kg) and xylazine (5 mg/kg) and transcardiacally perfused with 0.1 M phosphate buffer, pH 7.3, containing 2% paraformaldehyde and 2.5% glutaraldehyde. The 2-mm-thick slices were cut from the cerebellum and postfixed in 1% glutaraldehyde in phosphate buffer overnight at 4°C. The slices were then immersed for 1 h in OsO_4 0.5% in phosphate buffer. The 1 mm^3 blocks were cut in the cerebellum, dehydrated, and processed classically for embedding in araldite and ultramicrotomy. Ultrathin sections were counterstained with uranyl acetate. Fields

of view were randomly selected in ultrathin sections from several blocks (1 section/block) from each mouse.

Membrane sheets were prepared and processed as described previously (Gabel et al., 2015; Delavoie et al., 2021). In brief, carbon-coated Formvar films on nickel electron grids were inverted onto unstimulated or stimulated GrCs (Locke buffer containing 50 mM KCl) incubated with gold-conjugated AnxA5 for 10 min. To prepare membrane sheets, pressure was applied to the grids for 25 s, then grids were lifted so that the fragments of the upper cell surface adhered to the grids. These membrane sheets were then fixed in 2% paraformaldehyde for 10 min at 4°C, blocked in PBS with 1% BSA and 1% acetylated BSA and incubated with ~~antibodies~~ anti-GFP and anti-v-Glut1 antibodies (see Table 2) overnight at 4°C. Then the membranes were washed 6 times with PBS and incubated 3 h with 25 nm gold particle-conjugated goat anti-rabbit IgG and 10 nm gold particle-conjugated goat anti-guinea pig IgG (Table 2). These membrane portions were fixed in 2% glutaraldehyde in PBS, postfixed with 0.5% OsO4, dehydrated in a graded ethanol series, treated with hexamethyldisilazane (Sigma-Aldrich) and air dried. Transmission electron microscope (7500; Hitachi) equipped with camera (C4742-51-12NR; Hamamatsu Photonics) were used for acquisition. 20 to 40 fields of view were randomly taken and membrane patches labeled with vGlut1, GFP and/or AnxA5 were counted.

Morphometric analysis of electron microscopy slices

SVs, pre and post-synaptic membranes and boutons were manually selected or delineated using Icy bioimaging software. The density of SVs in the boutons and the shortest distance between SV and the pre-synaptic membrane were calculated. Synapse densities per field were also calculated and the mean distance of synaptic cleft were computed.

SynaptopHluorin live cell imaging

Imaging was performed with DIV6 to DIV7 GrCs as reported by (Nicholson-Fish et al., 2015). GrCs were removed from culture medium 48 to 72 h post transfection and repolarized in Imaging Buffer (see above) for 15 min. Coverslips were then mounted in an imaging chamber (Warner RC-21BRFS) supplied with a pair of embedded platinum wires allowing connection to a low impedance field stimulator (Digitimer, D330 MultiStim System). The chamber was placed on the stage of an inverted microscope (Zeiss AxioObserver Z1) equipped with either a sCMOS camera (Orca-FLASH4, Hamamatsu) or a Zeiss AxioCam506 and a control of focus

(Zeiss Definite Focus) to prevent drift. During recording, cells were continuously perfused with Imaging Buffer at 37°C. Synaptophysin-pHluorin (Syp-pH) transfected neurons were visualized with a Zeiss Plan Apochromat x40 oil-immersion objective (NA 1.4) at 475 +/- 28 nm excitation wavelength using 525 +/- 50 nm emission filter (LED light source SpectraX, Lumencor) or exciter 450-490 nm, beam splitter 495 nm, emitter 500-550 nm, Colibri 7 LED light source (Zeiss)). When specified, co-transfected mCherry expression was visualized using 555 +/- 28 nm excitation and 605 +/- 70 nm emission filters or exciter 538-652 nm, beam splitter 570 nm, emitter 570-640 nm. Neurons were stimulated with a train of action potentials (400 action potentials delivered at 40 Hz; 100 mA, 1-ms pulse width) and the acquisition sequence driven by MetaMorph Software (Molecular Devices) or Zeiss Zen2 software at 0.5 Hz frequency. At the end of the recording, cells were challenged with alkaline imaging buffer (50 mM NH_4Cl substituted for 50 mM NaCl) to reveal total pHluorin fluorescence. To protect neurons from photodamage and subsequently minimize fluorescent protein photobleaching, we restricted light exposure (using low light power and a 0.5Hz frequency). Photobleaching was evaluated by monitoring fluorescence stability in regions unaffected by stimulation (cell body when in the field of view or neuron extension without synapses if absent cell body). Photobleaching measurements appeared limited and more importantly comparable between conditions and accounts for roughly 12 % ± 2% of the fluorescence decay at 120 seconds. If, for any reason and despite automatic focus control, visible drift occurred during recordings, the field was excluded from the analysis. Quantification of the time-lapse series was performed using the Time Series Analyzer plugin for ImageJ and only synapses that responded to action potential stimulation were selected for the analysis. A circular region of interest (ROI, 1.8 μm diameter) was drawn around each spot characterized by a sudden rise in fluorescence. ROI was centered on the maximum fluorescence of the spot. The pHluorin fluorescence change in each spot was calculated as $\Delta F/F_0$, and n refers to the number of individual cells examined.

Synaptotagmin1 antibody uptake assay

Plscr1$^{+/+}$ and *Plscr1*$^{-/-}$ neurons were incubated for 30 min in culture medium (containing 25 mM KCl) in the presence of antibodies directed against the Syt1 luminal domain. Following incubation, neurons were washed and then fixed with ice-cold 4% PFA in PBS. The bound anti-Syt1 antibodies were visualized using Alexa Fluor® 555-conjugated goat anti-rabbit secondary antibodies. The neuronal network was outlined using hierarchical K-means thresholding

method applied to the Syt1 staining, and mean intensity within the resulting region of interest was computed. The signal intensity from *Plscr1*$^{-/-}$ neurons was normalized to that of *Plscr1*$^{+/+}$ neurons (± SEM). Experimental n refers to the number of individual cells examined.

Statistical analysis

Analysis was performed by using Microsoft Excel and GraphPad Prism (2018). All data passed normality test (Shapiro–Wilk test) and variance equality. A Student's t-test was performed for comparison between two datasets. Data were analysed by one-way analysis of variance (Anova) with Sidak's multiple comparison test when greater than two datasets. To compare fluorescence response over time or data with more than one variable, two-way Anova with Tukey's multiple comparison *post hoc* test was performed. All data are reported as mean ± standard error of the mean (SEM). To attest for similar SVs distribution, the Kolmogorov-Smirnov test was applied. Significance was set as *P < 0.05, **P < 0.01, ***P < 0.001. ns, non-significant

Databases

Preliminary information about *Plscr1* distribution in the mouse brain were obtained from the Allen brain atlas (https://mouse.brain-map.org/experiment/show/632487) and the Human brain atlas databases (https://www.proteinatlas.org/ENSG00000188313-PLSCR1/brain)

Results

PLSCR1 is expressed in cerebellar granular cells and localizes at synapses

PLSCR1 is expressed in a wide range of tissue including the brain (Wiedmer et al., 2000; Zhou et al., 2005). Mining in mouse brain databases revealed that the *Plscr1* transcript is barely detectable by *in situ* hybridization (Allen brain atlas) (Lein et al., 2007). However, it is expressed in the olfactory bulb, the cerebellum, the pons and medulla when using the more sensitive next generation sequencing (Human Protein Atlas) (Sjöstedt et al., 2020). To validate the expression profile of the PLSCR1 gene product in a specific area of the mouse brain, we dissected different brain areas to perform Western blots on tissue extracts from *Plscr1*$^{+/+}$ adult mice. As a negative control, we used cerebellar extracts from *Plscr1*$^{-/-}$. We confirmed that PLSCR1 is abundant in the cerebellum, with expression also observed in the olfactory bulb and midbrain albeit at lower levels. However, expression is barely detectable in all the other brain regions investigated (Fig. 1A). We therefore focused our studies on the cerebellum, which displayed the highest expression of PLSCR1 in mouse brain.

Since cerebellar granule cells (GrCs) account for 95% of cerebellum cells (D'Mello et al., 1993; Krämer and Minichiello, 2010), we first probed PLSCR1 expression in primary cultures of GrCs displaying high homogeneity. Western blot experiments revealed that PLSCR1 was expressed in GrCs cultured from *Plscr1*$^{+/+}$ mice but, as expected, absent from *Plscr1*$^{-/-}$ GrCs culture (Fig. 1B). We next analyzed PLSCR1 subcellular distribution. First, we prepared synaptosomes from mouse cerebellum to determine whether PLSCR1 was localized to synaptic terminals (Dunkley et al., 2008b). Compared to crude brain homogenate, PLSCR1 is enriched in synaptosomal fractions containing the post- and pre-synaptic markers PSD95 and Synaptotagmin-1 (Syt1), respectively (Fig. 1C). To further investigate the presence of PLSCR1 at synapses, we performed immunofluorescence on GrCs. Because of the lack of reliable antibodies to detect endogenous mouse PLSCR1 by immunofluorescence, we exogenously expressed GFP-tagged PLSCR1 and compared its distribution with specific markers of the pre-synaptic terminal, the vesicular glutamate transporter1 (vGlut1) and Synaptotagmin-1 (Syt1). GFP-PLSCR1 was found in GrC axons and colocalized with vGlut1 and Syt1, indicating that it is also present at the synapse (Fig. 1D). To further explore PLSCR1 localization, we performed immunogold electron microscopy (EM) analysis of native plasma membrane sheets of GrCs (Fig. 1E). Sheets were obtained by tearing off the plasma membrane at the dorsal surfaces of cells to examine, at high resolution, the associated molecules (Wilson et al., 2000; Gabel et al.,

2015). Synaptic components were retained by this method, since confocal analysis of recovered membrane pieces were stained for Synaptophysin and vGlut1. Electron microscopy analysis using secondary antibodies coupled to 10 nm gold particles, showed vGlut1 clusters on membrane patches of various size (Fig. 1E). Plasma membrane sheets from *Plscr1*$^{-/-}$ neurons expressing GFP-PLSCR1 were analyzed. Secondary antibodies coupled to 10- and 25- nm gold particles were used to reveal both the expression of vGLUT1 and GFP-PLSCR1 respectively (Fig. 1F). Gold particles of different size were found distributed over most membrane patches. In addition, GFP-PLSCR1 was localized close to vGlut1, with the majority of membrane patches containing vGlut1 also containing GFP-PLSCR1 (73% ± 13%; n=5 experiments). Altogether, our data indicate that GFP-PLSCR1 is associated to the plasma membrane of GrCs and is most likely enriched at the pre-synaptic terminal were vGlut1-positive SVs are located.

To determine whether *Plscr1* deletion could modify synaptic organization and/or characteristics, we performed morphometric analysis of sections from *Plscr1*$^{-/-}$ and *Plscr1*$^{+/+}$ cerebellum observed by transmission electron microscopy (Fig. 2A). GrC to Purkinje cell (PC) synapses from *Plscr1*$^{-/-}$ mice showed no significant differences in either synapse density per slice or SV density in synaptic boutons compared to *Plscr1*$^{+/+}$ mice (Fig. 2B). We measured the minimal distance separating each SV from the synaptic membrane facing the post-synaptic density, but found no significant differences in either the distribution of SVs (Fig. 2C) or the number of docked SVs (Fig. 2D). We did however note a slight decrease in synaptic length (Fig. 2E). The synaptic cleft, measured as the space separating the pre- and post-synaptic membranes, remained unchanged (Fig. 2E). Consequently, the absence of PLSCR1 has negligible impact on the structural organisation of GrC-PC synapses, suggesting that PLSCR1 does not influence developmental processes in the cerebellum.

GrCs stimulation triggers PLSCR1-dependent PS egress at synapses

Rapid activity-dependent transbilayer movement of PLs, mainly PS and PE, occurs in synaptosomes prepared from the electric organ of the electric ray, *Narke japonica* (Lee et al., 2000). We also demonstrated PLSCR1-dependent PS egress in chromaffin cells during exocytosis (Ory et al., 2013). We therefore asked whether stimulation of GrCs could lead to disruption of the plasma membrane asymmetry, and whether PLSCR1 was required for that process. To detect PS exposed to the extracellular leaflet of the plasma membrane, living GrCs were stimulated with a 50 mM KCl solution containing fluorescent AnnexinA5 (AnxA5), which

selectively binds to PS (Andree et al., 1990). GrCs were then fixed and stained for F-actin to delineate neuronal processes and to quantify AnxA5 staining. Compared to unstimulated neurons, depolarization of *Plscr1*$^{+/+}$ GrCs induced an increase in AnxA5 staining (Fig. 3A, B). Interestingly, the increase in AnxA5 staining was abrogated in stimulated *Plscr1*$^{-/-}$ GrCs (Fig. 3A, B) indicating that PLSCR1 was required for the activity-dependent translocation of PS to the extracellular leaflet.

AnxA5 staining organized as discrete spots along neuronal processes (Fig. 3A) suggesting that PS egress could preferentially occur at the synapse. To test this hypothesis, we took advantage of anti-Syt1 antibodies that recognize the luminal domain of the integral SV protein Syt1, which is transiently accessible from the extracellular space upon SV fusion with the plasma membrane (Fig. 3C). Incubating living GrCs with both fluorescent AnxA5 and anti-Syt1 antibodies showed that AnxA5 and Syt1 staining partially overlapped indicating that PS egress occurs at active synapses (Fig. 3C). We also prepared plasma membrane sheets of stimulated neurons to determine more precisely where PS egress occurs. Thus, *Plscr1*$^{+/+}$ GrCs were stimulated in the presence of gold-coupled AnxA5 and the distribution of AnxA5 was compared to vGlut1 on membrane sheets. As shown in Figure 3D, clusters of AnxA5 gold particles were found in membrane patches close to vGlut1 staining. Altogether, these data indicate that activity-dependent PS egress occurs at synapses, and that this egress requires expression of PLSCR1.

GFP-PLSCR1 restores PS egress in *Plscr1*$^{-/-}$ GrCs

To confirm that PLSCR1 is essential for PS egress, we performed rescue experiments. GFP-tagged PLSCR1 protein was expressed in *Plscr1*$^{-/-}$ GrCs and PS egress in response to KCl-dependent stimulation was analyzed on plasma membrane sheets. We observed GFP-PLSCR1 in membrane patches containing both vGlut1 and gold-coupled AnxA5 in response to cell stimulation (Fig. 4A). In addition, the percentage of membrane patches containing both vGlut1 and AnxA5 was comparable between *Plscr1*$^{+/+}$ neurons and *Plscr1*$^{-/-}$ neurons expressing GFP-PLSCR1 and increased in response to stimulation. In contrast, no increase was observed in *Plscr1*$^{-/-}$ GrCs (Fig. 4A). These data confirm that PLSCR1 is required for activity-dependent PS egress at synapses.

PLSCR1 is required for evoked synaptic transmission

A key unsolved question is whether PLSCR1activity is involved in neurotransmission. In the cerebellar cortex, GrCs convey high-frequency information (several hundreds of Hz) to

Purkinje cells (PCs) and molecular layer interneurons. GrC synapses stand out from most other synapse types by the striking ability to recruit reluctant SVs within milliseconds to sustain the release of glutamate at such extreme frequencies. This phenomenon underlies a large facilitation of glutamate release during paired-pulse stimulation elicited at high frequency (Miki et al., 2016; Doussau et al., 2017). GrCs can also be endowed with specific mechanisms optimizing the recycling of used SVs as the high facilitation of glutamate release observed during high frequency trains is maintained for hundreds of milliseconds (Doussau et al., 2017). Hence, to test whether PLSCR1 is required for these presynaptic properties of GrCs, we prepared acute cerebellar slices from *Plscr1*$^{+/+}$ and *Plscr1*$^{-/-}$ littermates in which we recorded excitatory postsynaptic currents (EPSCs) in PCs evoked by GrC axon stimulation (parallel fibres, PFs, Fig. 5A) with either twin stimuli (paired-pulse stimulation at 50 Hz) or high frequency trains. As expected in *Plscr1*$^{+/+}$ mice, amplitudes of EPSCs increased after the first stimulus (Fig. 5B). Furthermore, excitatory neurotransmission was facilitated and this facilitation was maintained during tens of stimuli (Fig. 5C). In contrast, in *Plscr1*$^{-/-}$ mice, paired-pulse facilitation was strongly reduced (mean paired-pulse ratio: 2.03 ± 0.7 for *Plscr1*$^{+/+}$ versus 1.59 ± 0.07 for *Plscr1*$^{-/-}$, *t*-test, p = 0.001, n= 7 for *Plscr1*$^{+/+}$ and n=8 for *Plscr1* $^{-/-}$). In addition, facilitation during the high frequency train was only transient, disappearing rapidly after the first ten stimuli (Fig. 5C).

The absence of observable abnormalities in the ultrastructure of *Plscr1*$^{-/-}$ GrC synapses (as shown in Figure 2) suggests that the presynaptic dysfunctions observed are unlikely to be caused by fewer SVs in GrC boutons or major anatomical defects. Instead, it is more likely that PLSCR1 plays a key role in facilitating the rapid recruitment of reluctant vesicles (exocytosis) and/or in the recycling of previously used SVs (endocytosis).

PLSCR1 is required for SV retrieval

To ascertain whether the effects observed on neurotransmission in the absence of PLSCR1 were due to altered SV exocytosis or endocytosis, we performed real-time monitoring of the genetically-encoded synaptophysin-pHluorin (Syp-pH) reporter. Syp-pH is widely used to report SV recycling since it responds to local pH changes occurring during SV exocytosis and endocytosis (Granseth et al., 2006; Nicholson-Fish et al., 2015; Jäpel et al., 2020). In resting conditions, as pHluorin faces the SV lumen, the fluorescence of Syp-pH is quenched by the acidic pH of the SV. Upon exocytosis, Syp-pH is exposed to the neutral extracellular medium, resulting in fluorescence unquenching, the quantification of which represents an assessment of

the extent of synaptic exocytosis. After termination of stimulation, Syp-pH fluorescence intensity decreases rapidly as it is retrieved by endocytic SVs, which quickly reacidify. As SV endocytosis is the rate limiting step in this fluorescence decrease, measurement of post-stimulus Syp-pH fluorescence decay is a reliable indicator of compensatory endocytosis (Sankaranarayanan and Ryan, 2000; Atluri and Ryan, 2006; Granseth et al., 2006; Egashira et al., 2015). *Plscr1*$^{+/+}$ or *Plscr1*$^{-/-}$ GrCs were transfected with Syp-pH and stimulated with a train of high-frequency action potentials (40Hz, 10s) to evoke robust exocytosis (Nicholson-Fish et al., 2015). Analysis of the fluorescence intensity profiles showed a fast rise in fluorescence upon stimulation for both genotypes (Fig. 6A, B) and a progressive return to the fluorescence baseline for *Plscr1*$^{+/+}$ GrCs. Although no significant differences in the amount of Syp-pH visiting the cell surface was observed (Fig. 6C), fluorescence decay was severely delayed in *Plscr1*$^{-/-}$ GrCs (Fig. 6B, D), suggesting that SV exocytosis was unaltered, but that endocytosis was impaired in the absence of PLSCR1. To confirm the requirement for PLSCR1 in SV endocytosis, we performed rescue experiments in *Plscr1*$^{-/-}$ GrCs using exogenous expression of the mCherry-tagged version of PLSCR1. Expression of exogenous PLSCR1 significantly restored the decay of fluorescence intensity (Fig. 6B, D), consistent with a role for PLSCR1 in compensatory endocytosis.

To further probe the role of PLSCR1 in SV endocytosis, we took advantage of GrC neuronal culture conditions, which uses mild depolarization (25 mM KCl) to maintain spontaneous synaptic activity required for GrC maturation and survival (D'Mello et al., 1993; Lawrie et al., 1993). To detect the spontaneous release of SVs and a potential subsequent defect in endocytosis, GrCs were incubated with culture medium containing antibodies directed against the luminal domain of Syt1. To reveal the amount of antibody remaining at the cell surface after continuous SV turnover, fluorescent secondary antibodies were added without cell permeabilization and their fluorescence intensity was quantified. In agreement with pHluorin experiments, surface Syt1 was increased by approximately 50% in *Plscr*$^{-/-}$ GrCs as compared to *Plscr1*$^{+/+}$ (Fig. 6E, F) providing further evidence that endocytosis of SV proteins was perturbed in the absence of PLSCR1.

Discussion

To sustain neurotransmission during elevated neuronal activity, a major reorganization of the neuronal plasma membrane has to occur to integrate the SV at the exocytic site and to subsequently retrieve lipids and proteins to replenish the vesicular pool (Binotti et al., 2021). While experimental evidence points to a major role for phosphoinositides and their metabolism in this process, the role of phospholipids such as PS and the regulation of their localisation has remained unexplored. Here, we provide the first evidence that PLSCR1 randomizes PS at synapses during heightened neuronal activity and that the resulting loss of plasma membrane asymmetry is dispensable for SVs exocytosis but necessary for compensatory SVs endocytosis. As a consequence of impaired vesicular pool replenishment, synaptic transmission at GrC to PC synapses in cerebellar acute slices displays accelerated depletion in the absence of PLSCR1. Therefore, we propose that PLSCR1 activity controls compensatory endocytosis in GrCs and contributes to sustain neurotransmission at high frequencies.

PLSCR1 and plasma membrane asymmetry disruption

Immunofluorescence and immunogold electron microscopy approaches revealed that, 1) PLSCR1 is enriched at synaptic terminals, and 2) PLSCR1 is required for activity-dependent PS egress at these synapses. This is the first evidence that PLSCR1 promotes shuffling of the lipid PS in neurons. PLSCR1 has been involved in lipid mixing both *in vitro* (Rayala et al., 2014) and in immune and chromaffin cells during regulated exocytosis (Kato et al., 2002; Ory et al., 2013). Our observation that PS egress is restricted to synapses indicates that PLSCR1 is probably activated locally as has been reported in chromaffin cells (Ory et al., 2013). In these cells, PS egress occurred only in the vicinity of exocytosis sites, despite PLSCR1 being homogeneously distributed at the plasma membrane (Ory et al., 2013). The low affinity of PLSCR1 for Ca^{2+} (Stout et al., 1998) together with the activity described here occurring only after neurotransmission suggests that PLSCR1 may only be activated when intracellular Ca^{2+} reaches a critical concentration. Typically, low affinity Ca^{2+} sensors must be localised close to the exocytic site, since the Ca^{2+} burst is spatially constrained within a microdomain at the presynaptic active zone (Neher and Sakaba, 2008). Our finding that PLSCR1 is required for SV endocytosis during periods of high activity, suggests that its activity-dependent triggering of PS redistribution must occur in or directly adjacent to the active zone. This latter region is

termed the periactive zone, and is where SV endocytosis is proposed to occur (Gad et al., 1998; Watanabe et al., 2013). It is particularly relevant in high frequency synapses, where rapid and repetitive stimulation leads to the accumulation of intracellular Ca^{2+} (Delvendahl et al., 2015). Thus, the localized activation of PLSCR1 and the ensuing PS redistribution play a crucial role in modulating synaptic function, especially in scenarios involving high-frequency synaptic activity.

How can the local loss of plasma membrane asymmetry control compensatory endocytosis?

In the absence of PLSCR1, PS translocation to the extracellular leaflet is blocked and SV endocytosis, as measured by the retrieval of Syp-pH and the amount of stranded Syt1 at the plasma membrane, is retarded dramatically. It is important to note that, while our analysis focuses on PS distribution to visualize membrane asymmetry changes, PLSCR1 itself is not selectively active towards PS but can redistribute various lipid types at the cell surface. Nonetheless, the unique physico-chemical properties of PS render it an attractive lipid for influencing membrane dynamics. Indeed, PS, along with phosphatidic acid (PA) and phosphoinositides (PIs) is an anionic phospholipids thought to contribute to the negative charge of the inner leaflet of the plasma membrane. Compared to PA and PIs, which represent only a minor fraction of the phospholipids present at the plasma membrane, PS is the predominant phospholipid, and its redistribution from one leaflet to the other should alter the biophysical properties of the plasma membrane (Yeung et al., 2008; Puchkov and Haucke, 2013). Depending on the timing of lipid scrambling relative to SV fusion, a local decrease of negative charges by local PS depletion may, for example, reduce the repulsive forces of opposing membrane to favor fusion between SVs and the plasma membrane (Davletov and Montecucco, 2010). However, the amount of Syp-pH visiting the plasma membrane during activity was unaffected in *Plscr1*$^{-/-}$ GrCs, suggesting that exocytosis was unaltered. In agreement, large dense core vesicle fusion was unaltered in chromaffin cells from *Plscr1*$^{-/-}$ mice (Ory et al., 2013).

An alteration in local membrane charge is not predicted to impact SV endocytosis. This is because accumulation of negatively charged phospholipids such as PtdIns(4,5)P_2 increase the recruitment of cytosolic proteins with positively charged residues (Kay and Fairn, 2019; Clarke et al., 2020) to favor membrane bending (Micheva et al., 2001; Puchkov and Haucke, 2013). In contrast, phospholipids scrambling may modify plasma membrane fluidity. Enriched in tightly packed sphingolipids, the outer plasma membrane leaflet is highly ordered and rigid (Gupta et

al., 2020; Lorent et al., 2020). Insertion of SVs that are highly enriched in cholesterol will most likely modify the lipid organization of the presynaptic plasma membrane (Takamori et al., 2006). Indeed, membrane cholesterol content affects lipid lateral self-diffusion, confines SV proteins and limits their diffusive behavior (Mercer et al., 2011; Dason et al., 2014; Byczkowicz et al., 2018; Wilson et al., 2020). PS and cholesterol are co-distributed in the inner leaflet of the plasma membrane and the local decrease of PS may also lead to a concomitant decrease in cholesterol content (Maekawa and Fairn, 2015) helping to fluidize the leaflet and clear the active zone. Alternatively, changes in PS distribution may unlock protein function. For example, PS shapes the transmembrane domain of synaptogyrin to bend membrane and generate SVs of homogeneous size. To achieve this, PS must be present simultaneously on both leaflets to induce a structural change in synaptogyrin, a function that is intrinsic to PLSCR1 (Yu et al., 2023). It remains to be seen whether proteins involved in endocytosis may have the same properties and the precise role of phospholipids egress needs to be further explored.

PLSCR1 and GrC neurotransmission

Synaptic plasticity allows for fast adaptation of synaptic strength to neuronal network activity, which is critical for information processing. This comes in two main modes: 1) functional plasticity, which changes the strength of the synapse by modifying signal transmission and 2) structural plasticity, which alters the number and/or shape of synapses, resulting in differential connectivity between neurons (Caroni et al., 2012). Morphometric analysis of *Plscr1*$^{-/-}$ cerebellum slices showed no major alteration within presynaptic terminals, suggesting that PLSCR1 may impair functional, rather than structural, plasticity. In the cerebellar cortex, GrC-PC synapses have to transmit sensorimotor information elicited at extreme frequencies (several hundred of Hz to kHz, (Rancz et al., 2007)). To do so, these synapses are endowed with specific presynaptic processes allowing a fast and sustained boost (facilitation) of the release neurotransmitters during bursts of high-frequency activities. The strikingly large facilitation that occurs during paired-pulse facilitation and during the first phase of high-frequency trains is underpinned by the ultra-fast recruitment of a pool of reluctant SVs that can only be mobilized by high-frequency activities (Miki et al., 2016; Doussau et al., 2017). This phenomenon is affected in *Plscr1*$^{-/-}$ GrC terminals, indicating that PLSCR1 activity control directly or indirectly the size of the reluctant pool and/or its recruitment. The presence of PLSCR1 is also required for the fast mobilization of recycling SVs that support the maintenance of a high level of facilitation during prolonged stimulations. Whether SV mobilization defects

are directly or indirectly related to the slowing down of SV endocytosis needs to be clarified. Furthermore, we cannot exclude alternative mechanisms underlying the facilitation defect as altered clearance of SV cargo from release sites or an increase in release probability resulting from compensatory mechanisms.

Interestingly, we detected PLSCR1 in the cerebellum and the olfactory bulb, two brain regions known to sustain high frequency stimulation. In contrast, PLSCR1 is barely detected in other brain area. PLSCR1 appears therefore a good candidate to play a specific role in high-frequency synaptic transmission by scrambling PLs at synapse, a fast way to modify plasma membrane properties.

References

Amir-Moazami O, Alexia C, Charles N, Launay P, Monteiro RC, Benhamou M (2008) Phospholipid Scramblase 1 Modulates a Selected Set of IgE Receptor-mediated Mast Cell Responses through LAT-dependent Pathway. Journal of Biological Chemistry 283:25514–25523.

Andree HA, Reutelingsperger CP, Hauptmann R, Hemker HC, Hermens WT, Willems GM (1990) Binding of vascular anticoagulant alpha (VAC alpha) to planar phospholipid bilayers. Journal of Biological Chemistry 265:4923–4928.

Atluri PP, Ryan TA (2006) The Kinetics of Synaptic Vesicle Reacidification at Hippocampal Nerve Terminals. J Neurosci 26:2313–2320.

Audo R, Hua C, Hahne M, Combe B, Morel J, Daien CI (2017) Phosphatidylserine Outer Layer Translocation Is Implicated in IL-10 Secretion by Human Regulatory B Cells. PLOS ONE 12:e0169755.

Bassé F, Stout JG, Sims PJ, Wiedmer T (1996) Isolation of an Erythrocyte Membrane Protein that Mediates Ca2+-dependent Transbilayer Movement of Phospholipid. J Biol Chem 271:17205–17210.

Bevers EM, Williamson PL (2016) Getting to the Outer Leaflet: Physiology of Phosphatidylserine Exposure at the Plasma Membrane. Physiological Reviews 96:605–645.

Binotti B, Jahn R, Pérez-Lara Á (2021) An overview of the synaptic vesicle lipid composition. Archives of Biochemistry and Biophysics 709:108966.

Bolz S, Kaempf N, Puchkov D, Krauss M, Russo G, Soykan T, Schmied C, Lehmann M, Müller R, Schultz C, Perrais D, Maritzen T, Haucke V (2023) Synaptotagmin 1-triggered lipid signaling facilitates coupling of exo- and endocytosis. Neuron in press Available at: https://www.cell.com/neuron/abstract/S0896-6273(23)00628-1 [Accessed September 22, 2023].

Bonnycastle K, Davenport EC, Cousin MA (2021) Presynaptic dysfunction in neurodevelopmental disorders: Insights from the synaptic vesicle life cycle. Journal of Neurochemistry 157:179–207.

Byczkowicz N, Ritzau-Jost A, Delvendahl I, Hallermann S (2018) How to maintain active zone integrity during high-frequency transmission. Neuroscience Research 127:61–69.

Caroni P, Donato F, Muller D (2012) Structural plasticity upon learning: regulation and functions. Nat Rev Neurosci 13:478–490.

Chanaday NL, Cousin MA, Milosevic I, Watanabe S, Morgan JR (2019) The Synaptic Vesicle Cycle Revisited: New Insights into the Modes and Mechanisms. J Neurosci 39:8209–8216.

Cheung G, Cousin MA (2011) Quantitative analysis of synaptic vesicle pool replenishment in cultured cerebellar granule neurons using FM dyes. J Vis Exp:3143.

Clarke RJ, Hossain KR, Cao K (2020) Physiological roles of transverse lipid asymmetry of animal membranes. Biochimica et Biophysica Acta (BBA) - Biomembranes 1862:183382.

Daleke DL (2003) Regulation of transbilayer plasma membrane phospholipid asymmetry. J Lipid Res 44:233–242.

Dason JS, Smith AJ, Marin L, Charlton MP (2014) Cholesterol and F-actin are required for clustering of recycling synaptic vesicle proteins in the presynaptic plasma membrane. The Journal of Physiology 592:621–633.

Davletov B, Montecucco C (2010) Lipid function at synapses. Current Opinion in Neurobiology 20:543–549.

Delavoie F, Royer C, Gasman S, Vitale N, Chasserot-Golaz S (2021) Transmission Electron MicroscopyMicroscopy and TomographyTomography on Plasma MembranePlasma membranes Sheets to Study Secretory Docking. In: Exocytosis and Endocytosis: Methods and Protocols (Niedergang F, Vitale N, Gasman S, eds), pp 301–309 Methods in Molecular Biology. New York, NY: Springer US. Available at: https://doi.org/10.1007/978-1-0716-1044-2_20 [Accessed September 22, 2023].

Delvendahl I, Jablonski L, Baade C, Matveev V, Neher E, Hallermann S (2015) Reduced endogenous Ca^{2+} buffering speeds active zone Ca^{2+} signaling. Proceedings of the National Academy of Sciences 112:E3075–E3084.

D'Mello SR, Galli C, Ciotti T, Calissano P (1993) Induction of apoptosis in cerebellar granule neurons by low potassium: inhibition of death by insulin-like growth factor I and cAMP. PNAS 90:10989–10993.

Doussau F, Schmidt H, Dorgans K, Valera AM, Poulain B, Isope P (2017) Frequency-dependent mobilization of heterogeneous pools of synaptic vesicles shapes presynaptic plasticity Slutsky I, ed. eLife 6:e28935.

Dunkley PR, Jarvie PE, Robinson PJ (2008a) A rapid Percoll gradient procedure for preparation of synaptosomes. Nat Protoc 3:1718–1728.

Dunkley PR, Jarvie PE, Robinson PJ (2008b) A rapid Percoll gradient procedure for preparation of synaptosomes. Nat Protoc 3:1718–1728.

Egashira Y, Takase M, Takamori S (2015) Monitoring of Vacuolar-Type H+ ATPase-Mediated Proton Influx into Synaptic Vesicles. J Neurosci 35:3701–3710.

Gabel M, Delavoie F, Demais V, Royer C, Bailly Y, Vitale N, Bader M-F, Chasserot-Golaz S (2015) Annexin A2–dependent actin bundling promotes secretory granule docking to the plasma membrane and exocytosis. The Journal of Cell Biology 210:785–800.

Gad H, Löw P, Zotova E, Brodin L, Shupliakov O (1998) Dissociation between Ca2+-triggered synaptic vesicle exocytosis and clathrin-mediated endocytosis at a central synapse. Neuron 21:607–616.

Granseth B, Odermatt B, Royle SJ, Lagnado L (2006) Clathrin-Mediated Endocytosis Is the Dominant Mechanism of Vesicle Retrieval at Hippocampal Synapses. Neuron 51:773–786.

Gupta A, Korte T, Herrmann A, Wohland T (2020) Plasma membrane asymmetry of lipid organization: fluorescence lifetime microscopy and correlation spectroscopy analysis[S]. Journal of Lipid Research 61:252–266.

Jäpel M, Gerth F, Sakaba T, Bacetic J, Yao L, Koo S-J, Maritzen T, Freund C, Haucke V (2020) Intersectin-Mediated Clearance of SNARE Complexes Is Required for Fast Neurotransmission. Cell Reports 30:409-420.e6.

Kato N, Nakanishi M, Hirashima N (2002) Transbilayer Asymmetry of Phospholipids in the Plasma Membrane Regulates Exocytotic Release in Mast Cells. Biochemistry 41:8068–8074.

Kay JG, Fairn GD (2019) Distribution, dynamics and functional roles of phosphatidylserine within the cell. Cell Commun Signal 17:1–8.

Kobayashi T, Menon AK (2018) Transbilayer lipid asymmetry. Current Biology 28:R386–R391.

Krämer D, Minichiello L (2010) Cell Culture of Primary Cerebellar Granule Cells. In: Mouse Cell Culture (Ward A, Tosh D, eds), pp 233–239 Methods in Molecular Biology. Totowa, NJ: Humana Press. Available at: http://link.springer.com/10.1007/978-1-59745-019-5_17 [Accessed December 15, 2021].

Lawrie AM, Graham ME, Thorn P, Gallacher DV, Burgoyne RD (1993) Synchronous calcium oscillations in cerebellar granule cells in culture mediated by NMDA receptors: NeuroReport 4:539–542.

Lee D-S, Hirashima N, Kirino Y (2000) Rapid transbilayer phospholipid redistribution associated with exocytotic release of neurotransmitters from cholinergic nerve terminals isolated from electric ray Narke japonica. Neuroscience Letters 291:21–24.

Lein ES et al. (2007) Genome-wide atlas of gene expression in the adult mouse brain. Nature 445:168–176.

Lorent JH, Levental KR, Ganesan L, Rivera-Longsworth G, Sezgin E, Doktorova M, Lyman E, Levental I (2020) Plasma membranes are asymmetric in lipid unsaturation, packing and protein shape. Nature Chemical Biology 16:644–652.

Maekawa M, Fairn GD (2015) Complementary probes reveal that phosphatidylserine is required for the proper transbilayer distribution of cholesterol. J Cell Sci 128:1422–1433.

Malacombe M, Ceridono M, Calco V, Chasserot-Golaz S, McPherson PS, Bader M-F, Gasman S (2006) Intersectin-1L nucleotide exchange factor regulates secretory granule exocytosis by activating Cdc42. The EMBO Journal 25:3494–3503.

Manich M, Boquet-Pujadas A, Dallongeville S, Guillen N, Olivo-Marin J-C (2020) A Protocol to Quantify Cellular Morphodynamics: From Cell Labelling to Automatic Image Analysis. In: Eukaryome Impact on Human Intestine Homeostasis and Mucosal Immunology (Guillen N, ed), pp 351–367. Cham: Springer International Publishing.

Maritzen T, Haucke V (2018) Coupling of exocytosis and endocytosis at the presynaptic active zone. Neuroscience Research 127:45–52.

Martin S, Pombo I, Poncet P, David B, Arock M, Blank U (2000) Immunologic Stimulation of Mast Cells Leads to the Reversible Exposure of Phosphatidylserine in the Absence of Apoptosis. Int Arch Allergy Immunol 123:249–258.

Mercer AJ, Chen M, Thoreson WB (2011) Lateral mobility of presynaptic L-Type calcium channels at photoreceptor ribbon synapses. Journal of Neuroscience 31:4397–4406.

Micheva KD, Holz RW, Smith SJ (2001) Regulation of presynaptic phosphatidylinositol 4,5-biphosphate by neuronal activity. Journal of Cell Biology 154:355–368.

Miki T, Malagon G, Pulido C, Llano I, Neher E, Marty A (2016) Actin- and Myosin-Dependent Vesicle Loading of Presynaptic Docking Sites Prior to Exocytosis. Neuron 91:808–823.

Neher E, Sakaba T (2008) Multiple Roles of Calcium Ions in the Regulation of Neurotransmitter Release. Neuron 59:861–872.

Nicholson-Fish JC, Kokotos AC, Gillingwater TH, Smillie KJ, Cousin MA (2015) VAMP4 Is an Essential Cargo Molecule for Activity-Dependent Bulk Endocytosis. Neuron 88:973–984.

Ory S, Ceridono M, Momboisse F, Houy S, Chasserot-Golaz S, Heintz D, Calco V, Haeberle A-M, Espinoza FA, Sims PJ, Bailly Y, Bader M-F, Gasman S (2013) Phospholipid Scramblase-1-Induced Lipid Reorganization Regulates Compensatory Endocytosis in Neuroendocrine Cells. J Neurosci 33:3545–3556.

Puchkov D, Haucke V (2013) Greasing the synaptic vesicle cycle by membrane lipids. Trends in Cell Biology 23:493–503.

Rancz EA, Ishikawa T, Duguid I, Chadderton P, Mahon S, Häusser M (2007) High-fidelity transmission of sensory information by single cerebellar mossy fibre boutons. Nature 450:1245–1248.

Rayala S, Francis VG, Sivagnanam U, Gummadi SN (2014) N-terminal Proline-rich Domain Is Required for Scrambling Activity of Human Phospholipid Scramblases. J Biol Chem 289:13206–13218.

Rysavy NM, Shimoda LMN, Dixon AM, Speck M, Stokes AJ, Turner H, Umemoto EY (2014) Beyond apoptosis: The mechanism and function of phosphatidylserine asymmetry in the membrane of activating mast cells. BioArchitecture 4:127–137.

Sankaranarayanan S, Ryan TA (2000) Real-time measurements of vesicle-SNARE recycling in synapses of the central nervous system. Nat Cell Biol 2:197–204.

Sjöstedt E et al. (2020) An atlas of the protein-coding genes in the human, pig, and mouse brain. Science 367:eaay5947.

Smrž D, Lebduška P, Dráberová L, Korb J, Dráber P (2008) Engagement of Phospholipid Scramblase 1 in Activated Cells: IMPLICATION FOR PHOSPHATIDYLSERINE EXTERNALIZATION AND EXOCYTOSIS. Journal of Biological Chemistry 283:10904–10918.

Stout JG, Zhou Q, Wiedmer T, Sims PJ (1998) Change in Conformation of Plasma Membrane Phospholipid Scramblase Induced by Occupancy of Its Ca^{2+} Binding Site. Biochemistry 37:14860–14866.

Suzuki J, Denning DP, Imanishi E, Horvitz HR, Nagata S (2013) Xk-Related Protein 8 and CED-8 Promote Phosphatidylserine Exposure in Apoptotic Cells. Science 341:403–406.

Suzuki J, Umeda M, Sims PJ, Nagata S (2010) Calcium-dependent phospholipid scrambling by TMEM16F. Nature 468:834–838.

Takamori S et al. (2006) Molecular Anatomy of a Trafficking Organelle. Cell 127:831–846.

Vitale N, Caumont A-S, Chasserot-Golaz S, Du G, Wu S, Sciorra VA, Morris AJ, Frohman MA, Bader M-F (2001) Phospholipase D1: a key factor for the exocytotic machinery in neuroendocrine cells. The EMBO Journal 20:2424–2434.

Watanabe S, Rost BR, Camacho-Pérez M, Davis MW, Söhl-Kielczynski B, Rosenmund C, Jorgensen EM (2013) Ultrafast endocytosis at mouse hippocampal synapses. Nature 504:242–247.

Wiedmer T, Zhou Q, Kwoh DY, Sims PJ (2000) Identification of three new members of the phospholipid scramblase gene family. Biochimica et Biophysica Acta (BBA) - Biomembranes 1467:244–253.

Wilson BS, Pfeiffer JR, Oliver JM (2000) Observing Fcεri Signaling from the Inside of the Mast Cell Membrane. Journal of Cell Biology 149:1131–1142.

Wilson KA, MacDermott-Opeskin HI, Riley E, Lin Y, O'Mara ML (2020) Understanding the Link between Lipid Diversity and the Biophysical Properties of the Neuronal Plasma Membrane. Biochemistry 59:3010–3018.

Wu L-G, Chan CY (2024) Membrane transformations of fusion and budding. Nat Commun 15:21.

Wu L-G, Hamid E, Shin W, Chiang H-C (2014) Exocytosis and Endocytosis: Modes, Functions, and Coupling Mechanisms. Annu Rev Physiol 76:301–331.

Yang H, Kim A, David T, Palmer D, Jin T, Tien J, Huang F, Cheng T, Coughlin SR, Jan YN, Jan LY (2012) TMEM16F Forms a Ca2+-Activated Cation Channel Required for Lipid Scrambling in Platelets during Blood Coagulation. Cell 151:111–122.

Yeung T, Gilbert GE, Shi J, Silvius J, Kapus A, Grinstein S (2008) Membrane Phosphatidylserine Regulates Surface Charge and Protein Localization. Science 319:210–213.

Yu T, Flores-Solis D, Eastep GN, Becker S, Zweckstetter M (2023) Phosphatidylserine-dependent structure of synaptogyrin remodels the synaptic vesicle membrane. Nat Struct Mol Biol 30:926–934.

Zachowski A (1993) Phospholipids in animal eukaryotic membranes: transverse asymmetry and movement. Biochemical Journal 294:1–14.

Zhao S, Ting JT, Atallah HE, Qiu L, Tan J, Gloss B, Augustine GJ, Deisseroth K, Luo M, Graybiel AM, Feng G (2011) Cell type–specific channelrhodopsin-2 transgenic mice for optogenetic dissection of neural circuitry function. Nature Methods 8:745–752.

Zhou Q, Ben-Efraim I, Bigcas J-L, Junqueira D, Wiedmer T, Sims PJ (2005) Phospholipid Scramblase 1 Binds to the Promoter Region of the Inositol 1,4,5-Triphosphate Receptor Type 1 Gene to Enhance Its Expression. Journal of Biological Chemistry 280:35062–35068.

Zhou Q, Zhao J, Stout JG, Luhm RA, Wiedmer T, Sims PJ (1997) Molecular Cloning of Human Plasma Membrane Phospholipid Scramblase A PROTEIN MEDIATING TRANSBILAYER MOVEMENT OF PLASMA MEMBRANE PHOSPHOLIPIDS. J Biol Chem 272:18240–18244.

Zhou Q, Zhao J, Wiedmer T, Sims PJ (2002) Normal hemostasis but defective hematopoietic response to growth factors in mice deficient in phospholipid scramblase 1. Blood 99:4030–4038.

Figure legends

Figure 1: PLSCR1 is enriched at synapses of GrCs of the cerebellum.

A, immunodetection of PLSCR1 protein by western blot in the olfactory bulb (Olf. Bulb), cortex (prefrontal (Ctx Pre), parietal (Ctx Par) and occipital (Ctx Occ)) striatum, hippocampus (Hippoc.), midbrain, pons, medulla and cerebellum (Cereb.) from *Plscr1*$^{+/+}$ mice. As a control, cerebellum of *Plscr1*$^{-/-}$ mice was used. Blot with short and longer exposure are shown. Actin is shown as a loading control. **B**, immunodetection of PLSCR1 protein by western blot in cultured GrCs. **C**, PLSCR1 is enriched in synaptosomes. Cerebella were homogenized, cell body removed by centrifugation and the resultant supernatant layered on a discontinuous Percoll gradient. Fractions were collected and probed for PLSCR1, the presynaptic marker SYT1 and the postsynaptic marker PSD95. F2 corresponds to the fraction enriched in membranes and fractions F3 and F4 enriched in synaptosomes were pooled and compared to crude extract (CE) loaded on gradient. **D**, confocal microscopy of GrCs transfected with expression vector coding for GFP-PLSCR1 and labeled for vGLUT1 and SYT1. Mask of synapses containing the three markers is shown. **E**, *Top:* principle of plasma membrane sheet preparation. Carbon- coated Formwar films on nickel EM grids (1) were inverted onto neurons grown on poly-L-lysine-coated coverslips and pressure is applied to the grid (2). Grids are then lifted (3), leaving fragments of plasma membrane (blue) and synapses containing docked SVs (red) on the grids (4). *Bottom left:* confocal images of GrCs stained for vGLUT1 (red) and SYNAPTOPHYSIN (green). *Bottom right:* representative electron micrograph of GrCs plasma membrane sheets labeled for vGLUT1 (10 nm gold particles, arrow). **F**, electron micrograph of plasma membrane sheets prepared from *Plscr1*$^{-/-}$ GrCs expressing GFP-PLSCR1. Immunolabeling of GFP and vGLUT1 were revealed with 25 nm (green arrows) and 10 nm (red arrows) gold particles respectively.

Figure 2: Morphometric analysis of cerebellum slices observed by transmission electron microscopy. A, representative electron micrographs of cerebellum from *Plscr1*$^{+/+}$ and *Plscr1*$^{-/-}$ mice showing synapses between GrC and Purkinje cell dendrites (PC, asterisks). Bar: 100 nm. **B**, synapses number in each field of view were counted (5 fields of 4 μm^2, n=3 mice) and the number of synaptic vesicles (SVs) counted and reported on the surface of a bouton for *Plscr1*$^{+/+}$ and *Plscr1*$^{-/-}$ mice (± SEM). **C**, the shortest distance between SVs and the presynaptic membrane facing the postsynaptic density were calculated. The graph represents the

distribution of mean number of SVs found according to their distance to the synapse. **D**, graph representing cumulative distribution of docked vesicles at GrC-PC synapse (distance <50 nm). **E**, the presynaptic and postsynaptic membranes were manually delineated. The length of the presynapse and the mean distance between the pre- and post-synapse were calculated (synaptic cleft size). Statistical significance was assessed using unpaired t-test or Kolmogorov-Smirnov test for distribution analysis. ns: non significant, * $p<0.05$. ($p=0.79$ and $p=0.788$ (B); $p=0.7453$ (C); $p=0.996$ (D); $p=0.0162$ and $p=0.2157$ (E)). More than 210 synapses from 3 mice were analyzed for each genotype.

Figure 3: **PLSCR1-dependent PS egress occurs at synapses**. **A**, cultured GrCs from *Plscr1*$^{+/+}$ or *Plscr1*$^{-/-}$ mice were stimulated for 10 min with 50 mM KCl or maintained under resting condition in the presence of 1µg/mL fluorescent AnxA5 (magenta). Cells were fixed, counterstained for nuclei (blue) and actin (yellow) and observed under a confocal microscope. **B**, quantification of AnxA5 mean intensity of *Plscr1*$^{+/+}$ or *Plscr1*$^{-/-}$ neurons stimulated for 10 min with 50 mM KCl or maintained under resting condition (10 fields of view per experiments (±SEM), n=3 independent experiments). **C**, scheme of Syt1 staining assay. Living *Plscr1*$^{+/+}$ or *Plscr1*$^{-/-}$ GrCs were incubated in culture medium containing 25 mM KCl, anti-Syt1 antibodies directed against the luminal domain of Syt1 and fluorescent AnxA5 (green). Cells were fixed and anti-Syt1 antibody revealed with fluorescent secondary antibody without cell permeabilisation to reveal Syt1 at the plasma membrane (red). Cells were observed under a confocal microscope and intensity profile along the depicted line is shown. **D,** representative electron micrograph of plasma membrane sheets prepared from GrCs stimulated for 10 min in the presence of gold-conjugated AnxA5. Labeling of AnxA5 and vGlut1 were revealed with 15 nm (green arrows) and 10 nm (red arrows) gold particles respectively. Enlargements are shown in insets 1 and 2. Statistical significance was assessed using 2 way ANOVA with Holm-Sidak *post hoc* test. ns: non significant, **, $p<0.01$; ***, $p<0.001$. At least 21 fields of view from 3 independent experiments were analyzed for each condition.

Figure 4: Overexpression of PLSCR1 restores PS egress in *Plscr1*$^{-/-}$ GrCs. A, representative electron micrograph of plasma membrane sheets prepared from *Plscr1*$^{-/-}$ GrCs expressing GFP-PLSCR1. Neurons were stimulated for 10 min with 50 mM KCl (S) or maintained under resting condition (R) in the presence of gold-conjugated AnxA5 (15 nm beads). Immunolabeling of vGlut1 and GFP were revealed with 10 nm (red arrows), 15 nm (blue arrows) and 25 nm (green

arrows) gold particles respectively. The graph represents the percentage of synapses (membrane patches vGlut1 positive) closely associated to AnxA5 beads. Each point represents the mean of 2 (PLSCR1$^{+/+}$) or 3 independent experiments (PLSCR1$^{-/-}$). In each experiment, 40 to 50 images per conditions were quantified. ns, non significant; ***, p<0.001

Figure 5: PLSCR1 is required to sustain synaptic transmission at high firing rates. A, schematic representing the connectivity in the cerebellar cortex and the position of the stimulating and recording electrodes. (GrC: granule cell; PC: Purkinje cell, PF: parallel fiber, ML: molecular layer). **B,** *Left:* representative EPSCs evoked by paired-pulse stimulation (50 Hz) of PFs recorded in *Plscr1*$^{+/+}$ and *Plscr1*$^{-/-}$ mice acute slices (black and red traces respectively). Thick lines correspond to averaged EPSCs of at least 10 successive EPSCs (thin lines). Lower traces correspond to normalized averaged EPSCs. *Right*: Box-plots showing the values of the paired-pulse ratio obtained in *Plscr1*$^{+/+}$ and *Plscr1*$^{-/-}$ acute slice. White and blue lines correspond to mean and median values respectively (± SEM). **C,** *Left:* representative recording traces evoked by PF stimulations at 100 Hz (50 pulses) and recorded in *Plscr1*$^{+/+}$ and *Plscr1*$^{-/-}$ mice acute slices (black and red traces respectively). *Right:* Mean values of normalized EPSC amplitude elicited by trains of stimulation at 100 Hz and recorded in *Plscr1*$^{+/+}$ and *Plscr1*$^{-/-}$ mice acute slices (black and red traces respectively, ± SEM)

Figure 6: PLSCR1 is required for efficient SVs endocytosis during high frequency stimulation of GrCs. A, representative images of GrCs transfected with Synaptophysin-pHluorin (Syp-pH) and stimulated with a train of 400 action potentials delivered at 40 Hz. Still images show *Plscr1*$^{+/+}$ and *Plscr1*$^{-/-}$ GrCs before stimulation, 30 s and 180 s after stimulation. Inset shows a representative time course of Syp-pH variation at a single synapse. **B**, average normalized time course of fluorescence response of Syp-pH represented as $\Delta F/F_0$ ± SEM (5 independent preparations, n≥15 neurons by condition) in *Plscr1*$^{+/+}$, *Plscr1*$^{-/-}$ GRCs and *Plscr1*$^{-/-}$ GrCs transfected with mCherry-PLSCR1. **C**, mean peak of Syp-pH response during stimulation. Maximum Syp-pH intensity after stimulation was normalized to the total amount of Syp-pH at synapse obtained after incubation of neurons with 50 mM NH_4Cl (± SEM). **D**, mean normalized intensity of Syp-pH fluorescence remaining after 2 min imaging (± SEM). ns: non significant; **, p<0.01. **E**, representative confocal images of anti-Syt1 antibody uptake experiments. *Plscr1*$^{+/+}$ or *Plscr1*$^{-/-}$ GrC neurons were incubated in culture medium containing 25 mM KCl and antibodies directed against the luminal domain of Syt1 for 30 min. Neurons

were fixed and stained for the presence of Syt1 at the plasma membrane. **F**, quantification of Syt1 fluorescence normalized to *Plscr1*$^{+/+}$ (3 independent experiments, 10 fields of view per experiment. *, $p<0.05$).

Extended data: Statistical analysis report of all experiments

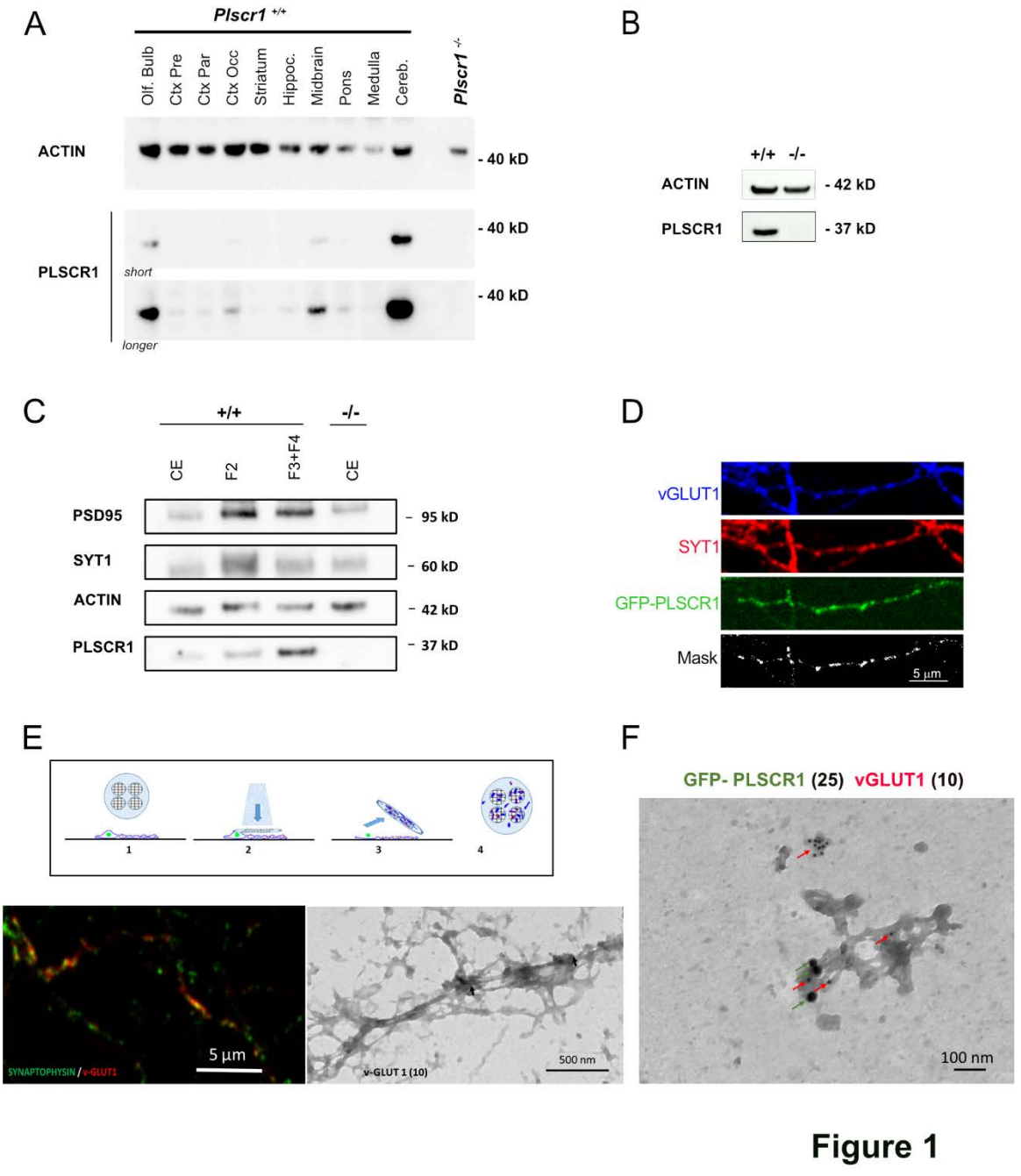
A
Plscr1 +/+
Olf. Bulb
Ctx Pre
Ctx Par
Ctx Occ
Striatum
Hippoc.
Midbrain
Pons
Medulla
Cereb.
Plscr1 -/-
ACTIN
- 40 kD
PLSCR1
short
- 40 kD
longer
- 40 kD
B
+/+ -/-
ACTIN
- 42 kD
PLSCR1
- 37 kD
C
+/+
-/-
CE
F2
F3+F4
CE
PSD95
- 95 kD
SYT1
- 60 kD
ACTIN
- 42 kD
PLSCR1
- 37 kD
D
vGLUT1
SYT1
GFP-PLSCR1
Mask
5 µm
E
1
2
3
4
SYNAPTOPHYSIN / v-GLUT1
5 µm
v-GLUT 1 (10)
500 nm
F
GFP- PLSCR1 (25) vGLUT1 (10)
100 nm

Figure 1

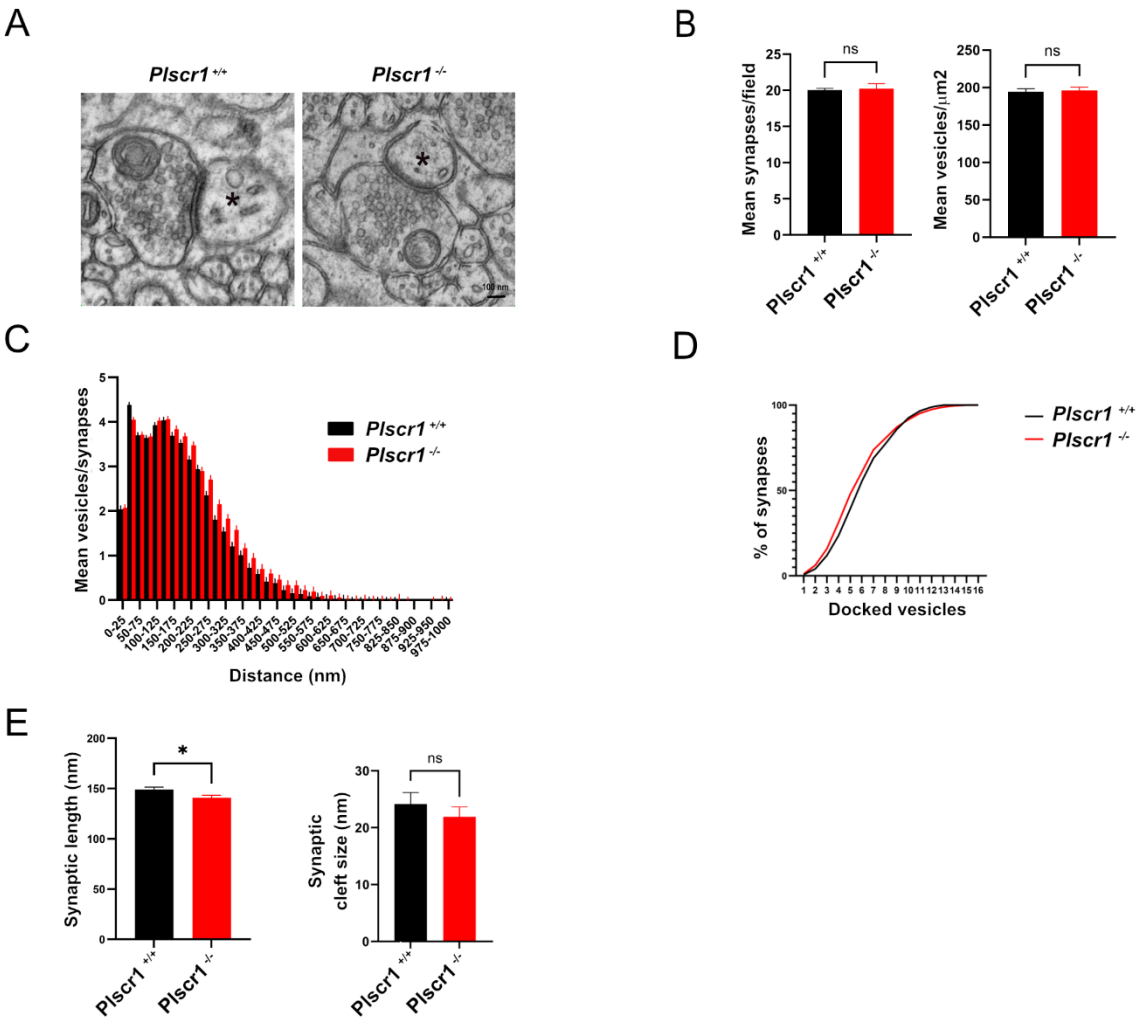
A
Plscr1 +/+
Plscr1 -/-
100 nm
B
Mean synapses/field
ns
Plscr1 +/+
Plscr1 -/-
Mean vesicles/μm2
ns
Plscr1 +/+
Plscr1 -/-
C
Mean vesicles/synapses
Plscr1 +/+
Plscr1 -/-
0-25
50-75
100-125
150-175
200-225
250-275
300-325
350-375
400-425
450-475
500-525
550-575
600-625
650-675
700-725
750-775
825-850
875-900
925-950
975-1000
Distance (nm)
D
% of synapses
Plscr1 +/+
Plscr1 -/-
Docked vesicles
E
Synaptic length (nm)
*
Plscr1 +/+
Plscr1 -/-
Synaptic cleft size (nm)
ns
Plscr1 +/+
Plscr1 -/-

Figure 2

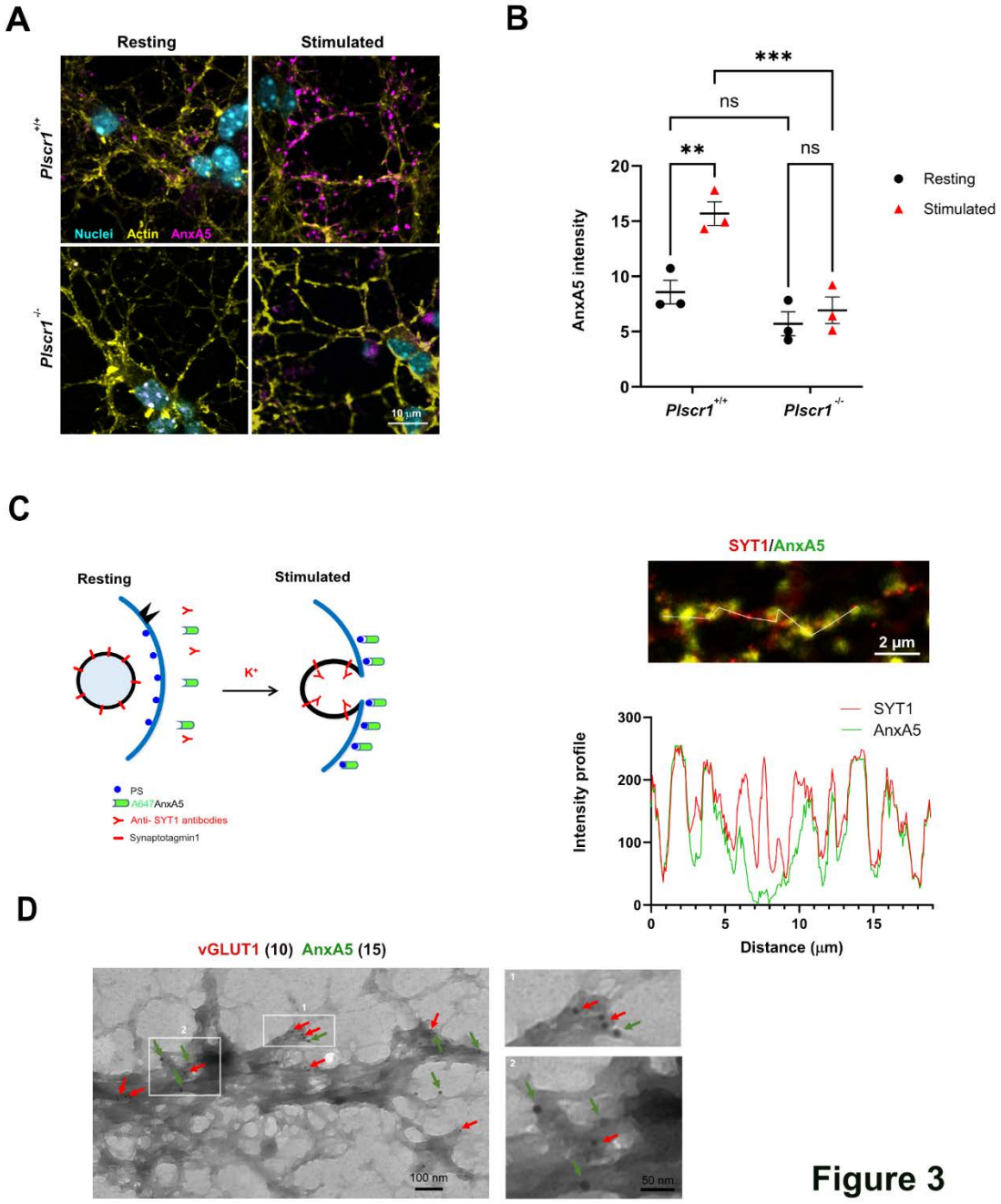
A
Resting
Stimulated
Plscr1+/+
Plscr1-/-
Nuclei
Actin
AnxA5
10 µm
B
***
ns
**
ns
AnxA5 intensity
20
15
10
5
0
Plscr1+/+
Plscr1-/-
Resting
Stimulated
C
Resting
Stimulated
K+
PS
A647AnxA5
Anti- SYT1 antibodies
Synaptotagmin1
SYT1/AnxA5
2 µm
SYT1
AnxA5
Intensity profile
300
200
100
0
0
5
10
15
Distance (µm)
D
vGLUT1 (10) AnxA5 (15)
1
2
100 nm
50 nm

Figure 3

A

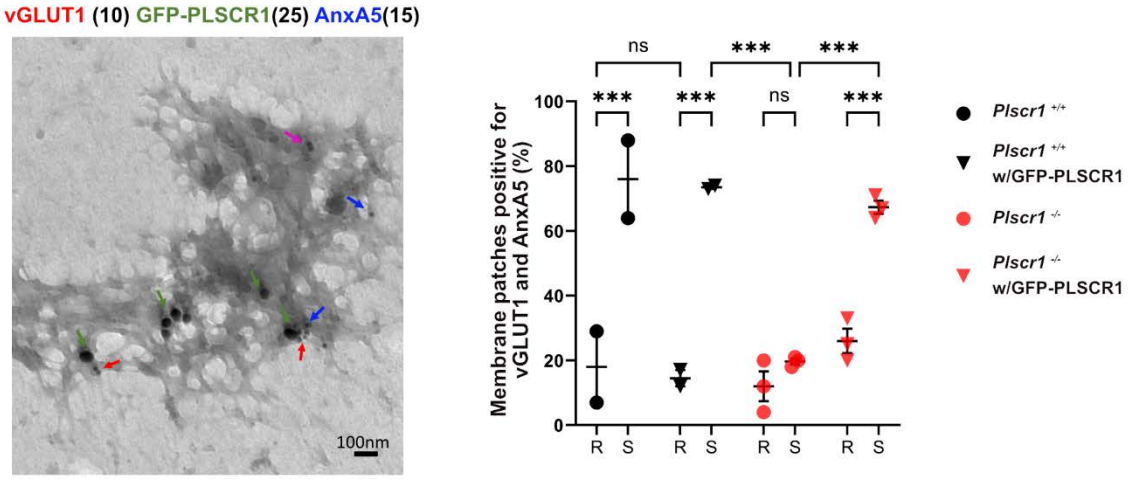
vGLUT1 (10) GFP-PLSCR1(25) AnxA5(15)
100nm
ns
***
***
***
***
ns
***
Membrane patches positive for vGLUT1 and AnxA5 (%)
100
80
60
40
20
0
R S R S R S R S
Plscr1 +/+
Plscr1 +/+ w/GFP-PLSCR1
Plscr1 -/-
Plscr1 -/- w/GFP-PLSCR1

Figure 4

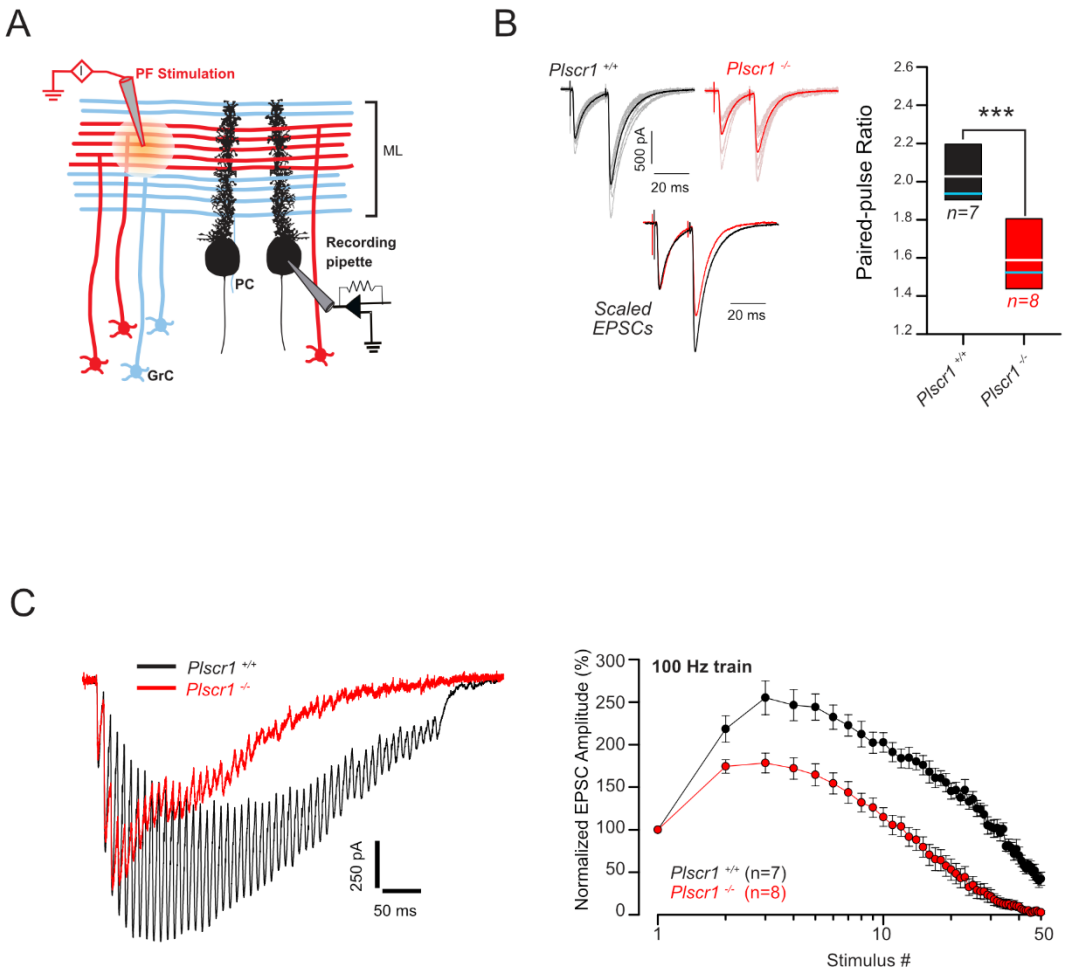
A
PF Stimulation
ML
Recording pipette
PC
GrC
B
Plscr1 +/+
Plscr1 -/-
500 pA
20 ms
Scaled EPSCs
20 ms
Paired-pulse Ratio
***
n=7
n=8
Plscr1 +/+
Plscr1 -/-
C
Plscr1 +/+
Plscr1 -/-
250 pA
50 ms
100 Hz train
Normalized EPSC Amplitude (%)
Plscr1 +/+ (n=7)
Plscr1 -/- (n=8)
Stimulus #

Figure 5

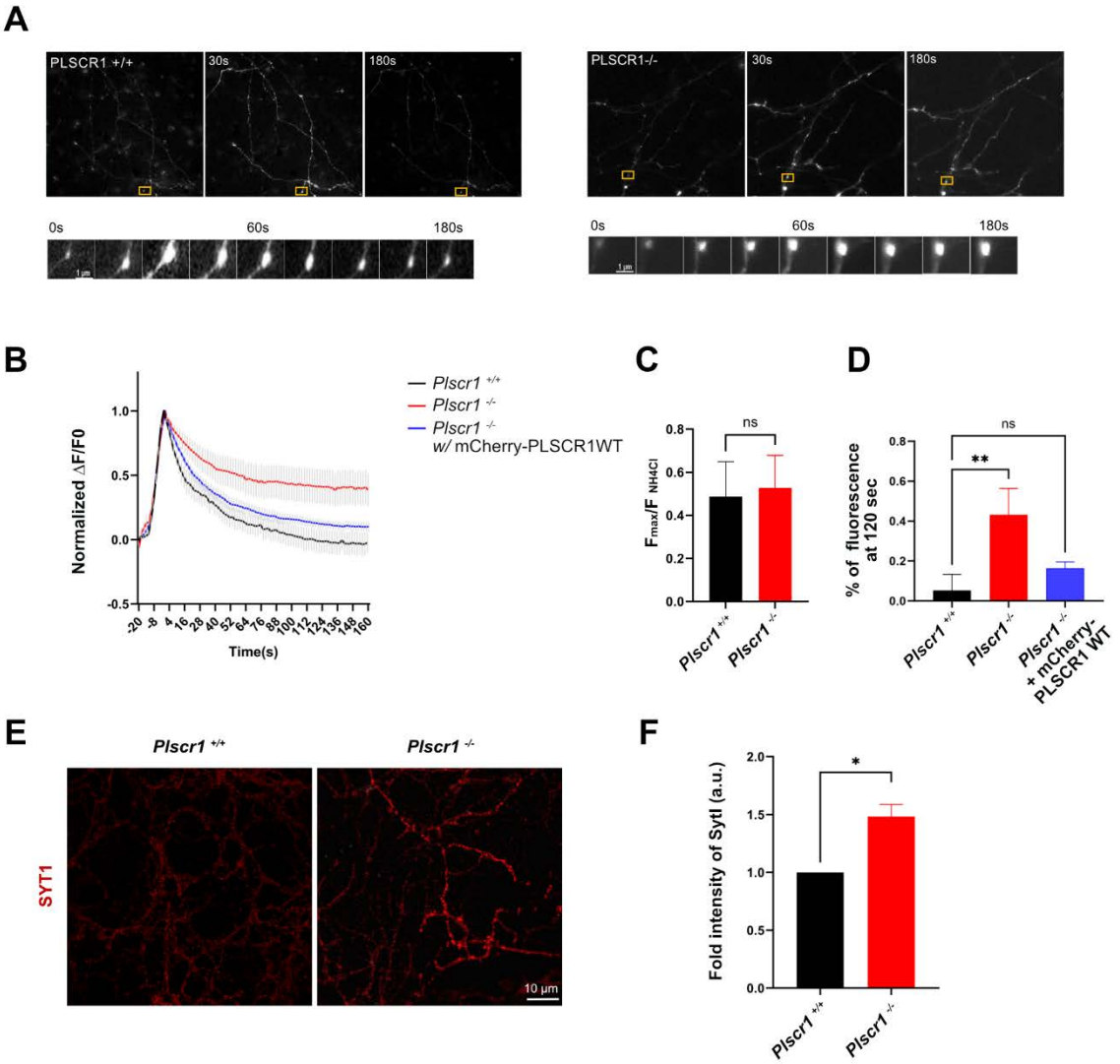
A
PLSCR1 +/+
30s
180s
0s
60s
180s
PLSCR1-/-
30s
180s
0s
60s
180s
B
Normalized ΔF/F0
Time(s)
Plscr1 +/+
Plscr1 -/-
Plscr1 -/-
w/ mCherry-PLSCR1WT
C
ns
Fmax/F NH4Cl
Plscr1 +/+
Plscr1 -/-
D
ns
**
% of fluorescence at 120 sec
Plscr1 +/+
Plscr1 -/-
Plscr1 -/- + mCherry-PLSCR1 WT
E
Plscr1 +/+
Plscr1 -/-
SYT1
10 μm
F
*
Fold intensity of SytI (a.u.)
Plscr1 +/+
Plscr1 -/-

Figure 6

Table Analyzed	synapse in fields	mean vesicle/ um2
Column B	PLSCR1 -/-	PLSCR1 -/-
vs.	vs,	vs,
Column A	PLSCR1 +/+	PLSCR1 +/+
Unpaired t test		
P value	0,79	0,7881
P value summary	ns	ns
Significantly different (P < 0.05)?	No	No
One- or two-tailed P value?	Two-tailed	Two-tailed
t, df	t=0,2847, df=4	t=0,2690, df=516
How big is the difference?		
Mean of column A	20	194,4
Mean of column B	20,21	196,1
Difference between means (B - A) ± SEM	0,2119 ± 0,7442	1,675 ± 6,229
95% confidence interval	-1,855 to 2,278	-10,56 to 13,91
R squared (eta squared)	0,01986	0,0001402
F test to compare variances		
F, DFn, Dfd	7,328, 2, 2	1,638, 299, 217
P value	0,2402	0,0001
P value summary	ns	***
Significantly different (P < 0.05)?	No	Yes
Data analyzed		
Sample size, column A	3	218
Sample size, column B	3	300

Table Analyzed	nombre moyen de vesicules/synapse 0-25	
Column A	PLSCR1 +/+	
vs.	vs,	
Column B	PLSCR1 -/-	
Kolmogorov-Smirnov test		
P value		0,7453
Exact or approximate P value?	Approximate	
P value summary	ns	
Significantly different (P < 0.05)?	No	
Kolmogorov-Smirnov D		0,1538

Table Analyzed	docked vesicle raw
Column A	WT
vs.	vs,
Column B	KO
Kolmogorov-Smirnov test	
P value	0,9996
Exact or approximate P value?	Approximate
P value summary	ns
Significantly different (P < 0.05)?	No
Kolmogorov-Smirnov D	0,125

Table Analyzed	synaptic length/animals	synaptic cleft /animals
Column B	PLSCR1-/-	PLSCR1-/-
vs.	vs,	vs,
Column A	PLSCR1+/+	PLSCR1 +/+
Unpaired t test		
P value	0,0162	0,2157
P value summary	*	ns
Significantly different (P < 0.05)?	Yes	No
One- or two-tailed P value?	Two-tailed	Two-tailed
t, df	t=3,034, df=8	t=1,469, df=4
How big is the difference?		
Mean of column A	147,7	24,15
Mean of column B	138,9	21,9
Difference between means (B - A) ± SEM	-8,811 ± 2,904	-2,248 ± 1,530
95% confidence interval	-15,51 to -2,113	-6,494 to 1,999
R squared (eta squared)	0,5349	0,3506
F test to compare variances		
F, DFn, Dfd	5,117, 4, 4	1,361, 2, 2
P value	0,1429	0,8473
P value summary	ns	ns
Significantly different (P < 0.05)?	No	No
Data analyzed		
Sample size, column A	5	3
Sample size, column B	5	3

Compare cell means regardless of rows and columns

Number of families	1
Number of comparisons per family	6
Alpha	0,05

Šídák's multiple comparisons test	Predicted (LS) mean diff,	95,00% CI of diff,	Below threshold?	Summary	Adjusted P Value
WT:Resting vs. WT:Stimulated	-6,028	-8,458 to -3,597	Yes	***	<0,001
WT:Resting vs. KO:Resting	3,784	1,448 to 6,121	Yes	***	<0,001
WT:Resting vs. KO:Stimulated	2,613	0,2769 to 4,950	Yes	*	0,02
WT:Stimulated vs. KO:Resting	9,812	7,588 to 12,04	Yes	***	<0,001
WT:Stimulated vs. KO:Stimulated	8,641	6,417 to 10,86	Yes	***	<0,001
KO:Resting vs. KO:Stimulated	-1,171	-3,291 to 0,9494	No	ns	0,6

Test details	Predicted (LS) mean 1	Predicted (LS) mean 2	Predicted (LS) mean diff,	SE of diff,	N1	N2	t	DF
WT:Resting vs. WT:Stimulated	9,132	15,16	-6,028	0,906	21	25	6,653	102
WT:Resting vs. KO:Resting	9,132	5,348	3,784	0,8708	21	30	4,346	102
WT:Resting vs. KO:Stimulated	9,132	6,519	2,613	0,8708	21	30	3,001	102
WT:Stimulated vs. KO:Resting	15,16	5,348	9,812	0,8288	25	30	11,84	102
WT:Stimulated vs. KO:Stimulated	15,16	6,519	8,641	0,8288	25	30	10,43	102
KO:Resting vs. KO:Stimulated	5,348	6,519	-1,171	0,7903	30	30	1,482	102

Compact letter display

WT:Stimulated	A
WT:Resting	B
KO:Stimulated	C
KO:Resting	C

Compare cell means with others in its row and its column

Number of families	6
Number of comparisons per row family	6
Number of comparisons per column family	1
Alpha	0,05

Uncorrected Fisher's LSD	Predicted (I	95,00% CI of diff,	Below threshold?	Summary	Individual P Value
R					
PLSCR1-/- vs. PLSCR1 -/- w/ GFP-PLSCR1	-14	-28,40 to 0,4008	No	ns	0,06
PLSCR1-/- vs. PLSCR1 +/+	-6	-22,10 to 10,10	No	ns	0,43
PLSCR1-/- vs. PLSCR1+/+ w/ GFP-PLSCR1	-2,5	-18,60 to 13,60	No	ns	0,74
PLSCR1 -/- w/ GFP-PLSCR1 vs. PLSCR1 +/+	8	-8,101 to 24,10	No	ns	0,3
PLSCR1 -/- w/ GFP-PLSCR1 vs. PLSCR1+/+ w/ GFP-PLSCR1	11,5	-4,601 to 27,60	No	ns	0,15
PLSCR1 +/+ vs. PLSCR1+/+ w/ GFP-PLSCR1	3,5	-14,14 to 21,14	No	ns	0,67
S					
PLSCR1-/- vs. PLSCR1 -/- w/ GFP-PLSCR1	-47,67	-62,07 to -33,27	Yes	***	<0,001
PLSCR1-/- vs. PLSCR1 +/+	-56,33	-72,43 to -40,23	Yes	***	<0,001
PLSCR1-/- vs. PLSCR1+/+ w/ GFP-PLSCR1	-53,83	-69,93 to -37,73	Yes	***	<0,001
PLSCR1 -/- w/ GFP-PLSCR1 vs. PLSCR1 +/+	-8,667	-24,77 to 7,434	No	ns	0,26
PLSCR1 -/- w/ GFP-PLSCR1 vs. PLSCR1+/+ w/ GFP-PLSCR1	-6,167	-22,27 to 9,934	No	ns	0,42
PLSCR1 +/+ vs. PLSCR1+/+ w/ GFP-PLSCR1	2,5	-15,14 to 20,14	No	ns	0,76
PLSCR1-/-					
R vs. S	-7,667	-22,07 to 6,734	No	ns	0,27
PLSCR1 -/- w/ GFP-PLSCR1					
R vs. S	-41,33	-55,73 to -26,93	Yes	***	<0,001
PLSCR1 +/+					
R vs. S	-58	-75,64 to -40,36	Yes	***	<0,001
PLSCR1+/+ w/ GFP-PLSCR1					
R vs. S	-59	-76,64 to -41,36	Yes	***	<0,001

Test details	Predicted (I	Predicted (LS) mea	Predicted (LS) mea	SE of diff,	N1	N2	t	DF
R								
PLSCR1-/- vs. PLSCR1 -/- w/ GFP-PLSCR1	12	26	-14	6,609	3	3	2,118	12
PLSCR1-/- vs. PLSCR1 +/+	12	18	-6	7,39	3	2	0,812	12
PLSCR1-/- vs. PLSCR1+/+ w/ GFP-PLSCR1	12	14,5	-2,5	7,39	3	2	0,338	12
PLSCR1 -/- w/ GFP-PLSCR1 vs. PLSCR1 +/+	26	18	8	7,39	3	2	1,083	12
PLSCR1 -/- w/ GFP-PLSCR1 vs. PLSCR1+/+ w/ GFP-PLSCR1	26	14,5	11,5	7,39	3	2	1,556	12
PLSCR1 +/+ vs. PLSCR1+/+ w/ GFP-PLSCR1	18	14,5	3,5	8,095	2	2	0,432	12
S								
PLSCR1-/- vs. PLSCR1 -/- w/ GFP-PLSCR1	19,67	67,33	-47,67	6,609	3	3	7,212	12
PLSCR1-/- vs. PLSCR1 +/+	19,67	76	-56,33	7,39	3	2	7,623	12
PLSCR1-/- vs. PLSCR1+/+ w/ GFP-PLSCR1	19,67	73,5	-53,83	7,39	3	2	7,285	12
PLSCR1 -/- w/ GFP-PLSCR1 vs. PLSCR1 +/+	67,33	76	-8,667	7,39	3	2	1,173	12
PLSCR1 -/- w/ GFP-PLSCR1 vs. PLSCR1+/+ w/ GFP-PLSCR1	67,33	73,5	-6,167	7,39	3	2	0,835	12
PLSCR1 +/+ vs. PLSCR1+/+ w/ GFP-PLSCR1	76	73,5	2,5	8,095	2	2	0,309	12
PLSCR1-/-								
R vs. S	12	19,67	-7,667	6,609	3	3	1,16	12
PLSCR1 -/- w/ GFP-PLSCR1								
R vs. S	26	67,33	-41,33	6,609	3	3	6,254	12
PLSCR1 +/+								
R vs. S	18	76	-58	8,095	2	2	7,165	12
PLSCR1+/+ w/ GFP-PLSCR1								
R vs. S	14,5	73,5	-59	8,095	2	2	7,289	12

Table Analyzed	peak heights WT vs PLSCR1KO
Column B	PLSCR1KO
vs.	vs,
Column A	WT
Unpaired t test	
P value	0,4959
P value summary	ns
Significantly different (P < 0.05)?	No
One- or two-tailed P value?	Two-tailed
t, df	t=0,6891, df=31
How big is the difference?	
Mean of column A	0,3551
Mean of column B	0,4159
Difference between means (B - A) ± SEM	0,06078 ± 0,08820
95% confidence interval	-0,1191 to 0,2407
R squared (eta squared)	0,01509
F test to compare variances	
F, DFn, Dfd	1,009, 15, 16
P value	0,9821
P value summary	ns
Significantly different (P < 0.05)?	No
Data analyzed	
Sample size, column A	17
Sample size, column B	16

Table Analyzed	recovery at 120 sec
Data sets analyzed	A-C

ANOVA summary	
F	4,612
P value	0,0149
P value summary	*
Significant diff. among means (P < 0.05)?	Yes
R squared	0,167

Brown-Forsythe test	
F (DFn, DFd)	6,352 (2, 46)
P value	0,0037
P value summary	**
Are SDs significantly different (P < 0.05)?	Yes

Bartlett's test	
Bartlett's statistic (corrected)	23,67
P value	<0,0001
P value summary	****
Are SDs significantly different (P < 0.05)?	Yes

ANOVA table	SS	DF	MS	F (DFn, DFd)	P value
Treatment (between columns)	1,236	2	0,618	F (2, 46) = 4,6	P=0,0149
Residual (within columns)	6,165	46	0,134		
Total	7,401	48			

Data summary	
Number of treatments (columns)	3
Number of values (total)	49

Table Analyzed	tagmin avg
Column B	PLSCR1 -/-
vs.	vs,
Column A	PLSCR1 +/+
Unpaired t test with Welch's correction	
P value	0,0447
P value summary	*
Significantly different (P < 0.05)?	Yes
One- or two-tailed P value?	Two-tailed
Welch-corrected t, df	t=4,568, df=2,000
How big is the difference?	
Mean of column A	1
Mean of column B	1,481
Difference between means (B - A) ± SEM	0,4811 ± 0,1053
95% confidence interval	0,02792 to 0,9343
R squared (eta squared)	0,9125
F test to compare variances	
F, DFn, Dfd	Infinity, 2, 2
P value	<0,0001
P value summary	****
Significantly different (P < 0.05)?	Yes
Data analyzed	
Sample size, column A	3
Sample size, column B	3